Fat body-derived cytokine Upd2 controls disciplined migration of tracheal stem cells in *Drosophila*

Pengzhen Dong[1,2], Yue Li[1,2,3], Yuying Wang[1,2], Qiang Zhao[1,2], Tianfeng Lu[6], Jian Chen[1,2], Tianyu Guo[1,2], Jun Ma[7,8], Bing Yang[5,*], Honggang Wu[3,*], Hai Huang[1,2,4,*]

1 Second Affiliated Hospital, and Department of Cell Biology, Zhejiang University School of Medicine. Hangzhou, Zhejiang Province 310058.

2 State Key Laboratory of Transvascular Implantation Devices, Hangzhou 310009, China.

3 Zhejiang Key Laboratory of Precision Diagnosis and Therapy for Major Gynecological Diseases, Women's Hospital, Zhejiang University School of Medicine. Hangzhou, Zhejiang Province 310058.

4 Zhejiang Provincial Key Laboratory of Genetic & Developmental Disorders, Zhejiang University School of Medicine. Hangzhou 311121.

5 MOE Laboratory of Biosystem Homeostasis and Protection and Life Sciences Institute, Zhejiang University, Hangzhou, 310058, China.

6 Department of Developmental Biology & Neuroscience, Washington University in St. Louis, Missouri, United States, 63108.

7 Center for Genetic Medicine, the Fourth Affiliated Hospital, Zhejiang University School of Medicine, Hangzhou, Zhejiang 310058, China.

8 Institute of Genetics, Zhejiang University International School of Medicine, Hangzhou, Zhejiang 310058, China.

*Correspondence: bingyang@zju.edu.cn; honggangwu@zju.edu.cn; haihuang@zju.edu.cn

Abstract

Coordinated activation and directional migration of adult stem cells are essential for maintaining tissue homeostasis. *Drosophila* tracheal progenitors are adult stem cells that migrate posteriorly along the dorsal trunk to replenish degenerating branches that disperse the FGF mitogen. However, it is currently unknown how the overall anterior-to-posterior directionality of such migration is controlled. Here we show that individual progenitor cells migrate together in a concerted, disciplined manner, a behavior that is dependent on the neighboring fat body. We identify the fat body-derived cytokine, Upd2, in targeting and inducing JAK/STAT signaling in tracheal progenitors to maintain their directional migration. Perturbation of either Upd2 production in fat body or JAK/STAT signaling in trachea causes aberrant bidirectional migration of tracheal progenitors. We show that JAK/STAT signaling promotes the expression of genes involved in planar cell polarity leading to asymmetric localization of Fat in progenitor cells. We provide evidence that Upd2 transport requires Rab5- and Rab7-mediated endocytic sorting and Lbm-dependent vesicle trafficking. Our study thus uncovers an inter-organ communication in the control of disciplined migration of tracheal progenitor cells, a process that requires vesicular trafficking of fat body-derived cytokine Upd2 and JAK/STAT signaling-mediated activation of PCP genes.

Introduction

Adult stem cells are multipotent cell populations which inhabit their niche but mobilize to initiate tissue reconstruction during organismal growth and regeneration. An intriguing feature of stem cells is their capability of migrating in a disciplined directionality towards locations undergoing reconstruction (Li and Clevers, 2010). Such a highly disciplined movement is critical for maintaining tissue homeostasis and is influenced by various niche-intrinsic signals and external stimuli, and its aberrancy causes diseases such as hypertrophy (Zhou et al., 2024). The damaged tissue or distant organs that elicit systemic signals promote the migration of adult stem cells (Jones and Wagers, 2008). In addition, interactions with other cell types, soluble factors (e.g. cytokines, growth factors, and hormones) and tissue stiffness collectively bolster the mobilization of stem cells (Fuchs and Blau, 2020). Despite growing appreciation of adult stem cells as a primary source for tissue regeneration, the mechanism governing directional stem cell migration remains yet to be elucidated.

Drosophila tracheal progenitors are a population of adult stem cells that rebuild the degenerating trachea during metamorphosis. The progenitor cells reside in Tr4 and Tr5 metameres and start to move along the tracheal branch towards sites of regeneration (Chen and Krasnow, 2014; Pitsouli and Perrimon, 2010). Movement of these progenitor cells follows a stereotypical anterior-to-posterior axis (Figure 1A), thus representing a suitable system to investigate mechanisms controlling the directionality of stem cell migration. The activation of tracheal progenitors is stimulated by the morphogen Branchless (Bnl), fly homolog of fibroblast growth factor (FGF) (Chen and Krasnow, 2014), and the insulin hormone (Li et al., 2022). Intercellular communication and synergy between organs also contribute to the branching morphogenesis (Perochon et al., 2021; Schottenfeld et al., 2010; Tamamouna et al., 2021). The functional role of the interactions between trachea and other organs in modulating tracheal progenitor behavior has been largely unknown.

Drosophila fat body is the functional analog of mammalian adipose tissue and the major organ sensing various hormonal and nutritional signals to orchestrate systemic growth, metabolism and stem cell maintenance (Sriskanthadevan-Pirahas et al., 2022).

Fat body produces regulatory molecules known as fat body signals (FBSs), which remotely affect the activity of other organs (Ingaramo et al., 2020; Zheng et al., 2016). For instance, the fat body-to-brain signals modulate insulin-like peptides production (Rajan and Perrimon, 2012), visual attention and sleep behavior (Ertekin et al., 2020). The *Drosophila* family of interleukin-6 (IL-6)-like cytokines consist of Unpaired (Upd, also called Outstretched), Upd2 and Upd3, and serve as mediators of systemic signaling. Whereas Upd1 and Upd3 derive from fly brain and plasmatocytes (Beshel et al., 2017; Woodcock et al., 2015), Upd2 is primarily produced by the fat body (Rajan et al., 2017), although muscle-derived Upd2 is also reported (Zhao and Karpac, 2017). The Upd proteins act as ligands which bind to a common GP130-like receptor, Domeless (Dome) on target cells (Agaisse et al., 2003; Chen et al., 2002). Upon association of ligands, the Dome receptors dimerize and recruit the non-receptor tyrosine kinase JAKs leading to their subsequent transactivation via phosphorylation. The transactivated JAKs then phosphorylate the tyrosine residues of their substrates, including the bound receptors and cytosolic STATs. The phosphorylation of STATs promotes their dimerization and nuclear translocation to activate transcriptional program (Darnell, 1997). JAK/STAT signaling requires the IL-6 cytokines (Heinrich et al., 2003), and is implicated in numerous cellular events including cell proliferation, differentiation, migration and apoptosis (O'Shea et al., 2002).

Here, we investigate molecular basis underlying directional stem cell migration using the *Drosophila* tracheal progenitors as a model. Our results identify a cytokine-mediated inter-organ communication between fat body and the progenitor cells that is necessary for their disciplined, directional migration. The directional migration of the progenitors relies on JAK/STAT signaling and its downstream targets of planar cell polarity (PCP) components. Importantly, the Upd2 cytokines derived from fat body are transported through vesicular trafficking to induce JAK/STAT signaling in tracheal progenitors. Our study reveals that tracheal progenitors establish migratory directionality as they exit their niches and that the disciplined migration of the progenitors depends on an inter-organ signaling originating from the fat body.

Results

Dependence of tracheal progenitors on the fat body

The fly tracheal progenitors are activated and move posteriorly along the dorsal trunk (DT) at the onset of pupariation (Figure 1A). We set out to delve into the underlying mechanisms of directional progenitor cell movement and tentatively surveyed organs that may coordinate this process. In *Drosophila*, the fat body resides anatomically in proximity with trachea (Figure 1B, C; Video 1) and is the principal reservoir for energy consumption. To determine whether the integrity of fat body is required for tracheal progenitors, we perturbed larval or pupal fat body by expressing pro-apoptotic cell death genes, *hid* and *reaper* (*rpr*), under the control of a fat body-specific driver, *lsp2*-Gal4 (Cherbas et al., 2003). Expression of *hid* and *rpr* in L3 stage impaired fat body integrity and adipocyte abundance, and generated slender larvae and pupae (Figure 1-figure supplement 1A-D). In these animals, the tracheal progenitors exhibited a sign of undisciplined migration and tended to move bidirectionally (Figure 1D-F), although their migration rate, cell number and proliferation remained unchanged (Figure 1-figure supplement 1E-H and Figure 3-figure supplement 1). The undisciplined bidirectional migration behavior of tracheal progenitors in fat body-defective animals is in stark contrast to control animals where the progenitors migrated unambiguously towards posterior (Figure 1D-D'' and Video 2). To gain a quantitative view of progenitor cell migration, we traced the movement of individual cells by time-lapse confocal imaging. At 2hr APF, tracheal progenitors from fat body deficit animals displayed a symmetrical distribution relative to the junction between dorsal trunk (DT) and transverse connective (TC), compared with an L-shape localization of niche-associated and migratory progenitors established by a posterior movement in control (Figure 1G-H'). Gauging the vector denoting the movement of each progenitor (Figure 1I-I') revealed that the traces of progenitor groups in fat body-depleted animals exhibited a fan-shaped pattern (Figure 1J, J'). Owing to this undisciplined movement, entropy of the system was notably elevated upon increased inconsistency of migration vectors (Figure 1K). The bidirectional migratory progenitors displayed longer territory as assessed by binarized direction

139 (Figure 1L). Collectively, these results suggest that fat body has an integral role in
140 maintaining the discipline of tracheal progenitor movement.
141
142 Upd2-JAK/STAT signaling between fat body and trachea
143 Since fat body impacts the behavior of tracheal progenitors, we next attempted to
144 investigate the signal between these two interdependent organs. For this purpose, we
145 first performed RNA sequencing (RNA-seq) analysis of tracheal progenitors from
146 aforementioned fat body defective flies. The results revealed a dramatical alteration of
147 transcriptional program in tracheal progenitors upon the perturbation of fat body
148 (Figure 2-figure supplement 1A, B). Interestingly, the functional cluster of 'cytokine
149 activity' showed prominent enrichment in the differentially expressed genes (DEGs)
150 in progenitors from *lsp2>rpr.hid* pupae (Figure 2A). This raised the possibility that
151 certain cytokine-responsive signaling was induced in tracheal progenitors and the
152 signaling was compromised by impairment of fat body. Therefore, we proceeded to
153 analyze the expression of genes responsive to cytokine signaling. Analyzing the RNA-
154 seq data revealed that the cytokine-dependent JAK/STAT and Dpp signaling were
155 notably up-regulated upon the activation of progenitors (Figure 2B). Importantly, fat
156 body depletion led to suppression of target genes of JAK/STAT, PI3K and Dpp
157 signaling in tracheal progenitors, suggesting their dependence on the function of fat
158 body (Figure 2C).
159 To evaluate the roles of these signaling proteins, we perturbed their expression in fat
160 body by the expression of RNAi constructs. Knockdown of candidates including some
161 cytokines specifically in fat body did not affect the direction of tracheal progenitor
162 migration (Figure 2-figure supplement 1C-J), except for *upd2*, whose depletion
163 phenocopied fat body ablation-induced bidirectional movement of tracheal
164 progenitors (Figure 2D-F and Video 3). These results suggest a role of fat body-
165 produced Upd2 in remotely regulating the tracheal progenitors.
166 Then, we performed surface proteome *in vivo* (Li et al., 2020) to investigate the
167 spectrum of molecules received by trachea (Figure 2-figure supplement 2). The
168 trachea-associated proteins were biotinylated through a reaction mediated by a

169 membrane-tethered horse radish peroxidase (HRP-CD2) (Figure 2-figure supplement
170 2A-D). Of the 1684 streptavidin-precipitated proteins captured by mass spectrometry
171 (Figure 2G), a functional cluster enriched for receptor signaling via JAK/STAT was
172 identified (Figure 2H). The JAK/STAT pathway is one of the principal cellular
173 signaling that responds to Upd2 ligand (Hombria et al., 2005). *Drosophila* JAK/STAT
174 signaling is well-conserved (Arbouzova and Zeidler, 2006; Zeidler et al., 2000) and
175 comprises a single JAK (Hopscotch, Hop) and one STAT (Stat92E), in contrast to a
176 handful of homologues (four JAK and seven STAT genes) found in mammals.
177 Domeless (Dome), the receptor for JAK/STAT pathway, exhibited pronounced
178 expression in the tracheal progenitors (Figure 2-figure supplement 2E). To test if these
179 Dome receptors actively interact with their ligands, we adapted a technique to monitor
180 ligand-receptor interaction *in vivo* (Michel et al., 2011) and constructed a Dome
181 variant (DIPF) which only fluoresces in the ligand-binding and phosphorylated state
182 (Figure 2I). The signal of this DIPF reporter was detected in both larval fat body and
183 salivary gland (Figure 2-figure supplement 2F,H), which is consistent with active JAK
184 signaling implicated in the development of the tissues (Chakrabarti et al., 2016;
185 Krautz et al., 2020). When expressed in the tracheal system, DIPF displayed robust
186 fluorescent signal in the tracheal progenitors (Figure 2J). These data suggest that
187 receptor signaling of JAK/STAT is active in the tracheal progenitors.
188 To analyze the functional importance of JAK/STAT signaling in tracheal progenitors,
189 we perturbed the principal components of this signaling, namely the receptor Dome,
190 signal transducer Hop or the downstream transcription factor Stat92E, by *btl*-Gal4-
191 driven expression of RNAi constructs. Under these conditions in which JAK/STAT
192 pathway is compromised, the tracheal progenitors aberrantly migrated anteriorly,
193 which is reminiscent of *upd2* loss-of-function in the fat body (Figure 3A-E, Video 4
194 and Figure 3-figure supplement1A-D). The aberrant anterior migration of tracheal
195 progenitors upon perturbation of JAK/STAT components led to incomplete
196 regeneration of airway and impairment of tracheal integrity and caused melanization
197 in the trachea (Figure 3-figure supplement 1E-I). In agreement with genetic
198 perturbation of JAK/STAT signaling, pharmacological inhibition of JAK by a small-

199 molecule inhibitor, Tofacitinib (Palmroth et al., 2021), also triggered bidirectional
200 movement of tracheal progenitors (Figure 3F-H). The bidirectional movement was not
201 due to excessive progenitors or crowding (Figure 3-figure supplement 2A).
202 Concurrently, the activity of JAK/STAT pathway, as assessed by the Stat92E-GFP
203 reporter (Bach et al., 2007), was substantially impaired when components of the
204 pathway were depleted (Figure 3-figure supplement 2B-E, J). To determine whether
205 the tracheal JAK/STAT signaling depends on fat body-derived Upd2, we depleted
206 Upd2 in fat body and observed that Stat92E-GFP signal in tracheal progenitors was
207 severely decreased, suggesting that JAK/STAT signaling in the trachea requires fat
208 body-produced Upd2 (Figure 3-figure supplement 2F, G, J). Consistently, inhibition of
209 JAK/STAT signaling using Tofacitinib reduced the expression of Stat92E-GFP (Figure
210 3-figure supplement 2H-J). Taken together, these observations suggest that Upd2-
211 responsive JAK/STAT signaling in the trachea is essential for the disciplined
212 migration of progenitors.
213
214 Genes regulated by JAK/STAT signaling in the trachea
215 To gain a comprehensive understanding of the molecular details underlying the
216 discipline of tracheal progenitor migration, we conducted genomic chromatin
217 immunoprecipitation (ChIP-seq) to identify loci bound by Stat92E which functions as
218 the transcription factor of JAK/STAT pathway. This revealed a total of 21312 Stat92E
219 binding peaks, ~95.7% of which located within 2 kb of transcription start sites (TSSs)
220 of annotated genes (Figure 4-figure supplement 1A). In particular, 86% of the peaks
221 (18328 peaks) were enriched either in promoter regions or within gene bodies, and
222 66.1% of the peaks (13490 peaks) resided near the 5′ ends of annotated genes, namely
223 in the promoter regions, first exons and first introns (Figure 4-figure supplement 1B,
224 C). GO analysis of putative target genes of Stat92E identified one cluster associated
225 with establishment of planar polarity (Figure 4A). In line with this, the functional
226 class associated with establishment of planar polarity was also abundantly represented
227 among the differentially expressed genes (DEGs) upon the activation of tracheal
228 progenitors in larval-pupal transition (Figure 4B). Notably, Stat92E binding was

229 detected in the promoters and intronic regions of genes functioning in distal-to-
230 proximal signaling (Cho and Irvine, 2004), such as *dachsous* (*ds*), *four-jointed* (*fj*), *fz*,
231 *stan*, *Vang* and *fat2* (Figure 4C). Additionally, Stat92E occupied in the promoter
232 regions of *crb* and *yurt,* two genes involved in apical-basal polarity and tracheal tube
233 growth (Laprise et al., 2006; Schottenfeld-Roames and Ghabrial, 2012; Schottenfeld-
234 Roames et al., 2014) (Figure 4-figure supplement 1D). The enrichment of Stat92E in
235 the promoters and/or regulatory regions of these putative targets was confirmed by
236 ChIP-qPCR (Figure 4-figure supplement 1E).
237 To further validate these putative Stat92E targets and investigate their dependence on
238 JAK/STAT signaling, we analyzed their expression from several fosmid transgenes
239 which have a GFP tag fused to *ds*, *fj* or *ft* and express at endogenous levels. Ds and Fj
240 were abundant in the progenitor cells, but were vastly reduced upon depletion of
241 *dome*, *hop* or *stat92E*, suggesting that they are regulated by JAK/STAT pathway
242 (Figure 4D-M). Furthermore, it is reported that the function of Ft is influenced by
243 cell-autonomous increase of Ds level and its protein level is enhanced by Ds reduction
244 (Ambegaonkar et al., 2012; Matakatsu and Blair, 2004), which is also evidenced by
245 our analysis using *dsRNAi* and *UAS-ds* in the tracheal progenitors (Figure 4-figure
246 supplement 2A-D). In accordance with this notion, the level of Ft, as assayed by the
247 Ft-GFP reporter, was elevated by the reduction of JAK/STAT signaling (Figure 4N-
248 R). We also analyzed GFP-tagged fosmid transgenes of *fat2, crb* and *yurt* and found
249 that they were discernably reduced upon impairment of JAK/STAT signaling,
250 suggesting that they are also regulated by JAK/STAT pathway (Figure 4-figure
251 supplement 1F-T). Additionally, the transcription of *ds*, *fj*, *ft*, *fat2*, *crb*, and *yurt* was
252 compromised by expression of *stat92ERNAi* (Figure 4-figure supplement 1U). In sum,
253 these results suggest that JAK/STAT promotes components involved in the
254 establishment of polarity in tracheal cells.
255
256 <u>The roles of JAK/STAT targets in the disciplined migration</u>
257 To evaluate the functional roles of the polarity proteins in tracheal progenitor
258 migration, we perturbed their expression in the tracheal progenitors by expressing

259 RNAi against *ds*, *ft* or *fj*, which were identified by ChIP-seq as the targets of
260 JAK/STAT. In these flies, tracheal progenitors exhibited bidirectional movement,
261 which is reminiscent of the impairment of JAK/STAT signaling (Figure 5A-E and
262 Video 5). Similar observations were obtained by over-expression of *ft* or *ds* in the
263 trachea (Figure 5-figure supplement 1A-D), consistent with previous reports that both
264 loss- and gain-of-function of PCP components disrupt the planar cell polarity (Adler
265 et al., 2000; Tree et al., 2002; Vinson and Adler, 1987). The disciplined migration of
266 tracheal progenitors was also impaired by the expression of *fat2RNAi*, *crbRNAi*,
267 *yurtRNAi* or *scbRNAi* (Figure 5-figure supplement 1E-I), but was not affected by
268 perturbation of molecules involved in cell adhesion such as Enabled (Ena), Fak, E-
269 cadherin and Robo2 (Figure 5-figure supplement 1J).
270 Migratory cells generate protrusions at the leading edge to initiate movement (Cetera
271 et al., 2014). The normal posteriorly migrating tracheal progenitors extend protrusions
272 towards the migratory directions (Figure 5-figure supplement 2A), but in the
273 bidirectionally moving progenitors in which *upd2* in fat body was perturbed,
274 extensive filopodia were projected from both the anterior and posterior fronts (Figure
275 5-figure supplement 2B, C), indicating that the aberrantly anteriorly moving
276 progenitors may adopt the identity as those moving posteriorly. Bidirectionally
277 migrating progenitors induced by perturbation of JAK/STAT signaling did not alter
278 the expression of the tracheal inducer, *branchless* (*bnl*) (Figure 5-figure supplement
279 2D, E). Further analysis revealed that the progenitors exhibited elevated levels of Ft at
280 the leading edge where they attached to dorsal trunk (DT) (Figure 5F-G).
281 Accordingly, progenitors that underwent bidirectional movement exhibited
282 pronounced abundance of Ft at both the anterior and posterior frontal edges (Figure
283 5H-J). To further evaluate the functional roles of Ft-Ds-Fj module in disciplined
284 migration, we utilized the high-mobility carcinoma cells, SKOV-3, and found that
285 perturbation of Fj that phosphorylates the extracellular cadherin domains of both Ft
286 and Ds and modifies their heterophilic binding (Thomas and Strutt, 2012), Ft or Ds
287 concurrently displayed compromised directionality and reduced consistency of
288 movement in a two-dimensional culture (Figure 5K-M and Figure 5-figure

289 supplement 3). Together with the results in previous sections, these observations
290 suggest that the activated tracheal progenitors establish a disciplined migration
291 through the asymmetrical distribution of polarity proteins which is directed by an
292 Upd2-JAK/STAT signaling stemming from the remote organ of fat body.
293
294 Upd2 in the fat body-produced vesicle
295 Besides the JAK/STAT signaling, another functional class enriched for vesicle-
296 mediated transport was prominent from our surface proteome analysis of the trachea
297 (Figure 2H). A series of components that function in vesicle trafficking were
298 identified. It has been reported that IL-6 cytokines tend to be encapsulated in
299 secretory vesicles (Kandere-Grzybowska et al., 2003; Verboogen et al., 2018). To
300 visualize Upd2 production and investigate its transportation kinetics, an upd2-
301 mCherry transgene was developed and expressed under the control of *lsp2*-Gal4,
302 which enabled tracking the dynamics of Upd2 in fat body (Figure 6A). In agreement
303 with Upd2 being transported through vesicles, administration of L3 larvae with
304 Brefeldin A (BFA), which pharmacologically inhibits vesicle formation and transport,
305 sequestered Upd2 proteins in fat body (Figure 6B, C). To track the destination of the
306 Upd2-containing vesicles, we examined mCherry signals in adjacent tissues and
307 detected considerable amount of Upd2 puncta in the tracheal progenitors (Figure 6D).
308 BFA treatment reduced Upd2-mCherry puncta in the tracheal progenitors, suggesting
309 that tracheal progenitors receive vesicular Upd2 from the fat body (Figure 6E, F).
310 Perturbation of Grasp65, a Golgi reassembly stacking protein previously implicated in
311 Upd2 secretion (Rajan et al., 2017), also led to sequestration of Upd2-containing
312 vesicles in fat body (Figure 6G, H, J). The vesicle formation, function and
313 extracellular movement are dependent on the tetraspanin superfamily proteins
314 (Andreu and Yanez-Mo, 2014). We surveyed all the tetraspanin orthologs in fly for
315 potential roles in Upd2 vesicle formation and transport. When expressing *lbmRNAi* in
316 fat body, Upd2-containing vesicles were vastly increased (Figure 6I, J). Meanwhile,
317 perturbation of vesicle secretion or transport by expressing *grasp65RNAi* or *lbmRNAi*
318 in fat body eliminated the presence of fat body-origin Upd2 in the trachea, suggesting

319 that fat body-produced Upd2-containing vesicles function cell non-autonomously and
320 contribute to other tissues/organs (Figure 6K-N). It should be noted that knockdown
321 of *upd2* in the trachea did not alter the discipline of tracheal progenitor migration
322 (Figure 2-figure supplement 1K-M). Collectively, these results suggest that fat body-
323 produced Upd2 undergoes vesicle-mediated trafficking.
324
325 <u>The vesicular transport in JAK/STAT signaling</u>
326 The results in previous section suggest that the ligand of JAK/STAT signaling is
327 transported in a manner that depends on vesicle trafficking. To validate the role of fat
328 body-produced vesicles in inter-organ signaling, we used genetic and pharmacological
329 tools to perturb different processes of vesicle trafficking in fat body and monitored
330 JAK/STAT signaling in the tracheal progenitors. Expression of *grasp65RNAi* in fat
331 body reduced the activity of JAK/STAT signaling in the trachea, as assessed by the
332 Stat92E-GFP reporter (Figure 7A, B). Similarly, RNAi targeting expression of *lbm* in
333 fat body vanished JAK/STAT signal transduction in the trachea (Figure 7C). Rab
334 GTPases coordinate vesicle trafficking and production (Stenmark, 2009) and have
335 been shown to play pivotal roles in the regulation of intracellular trafficking of FGFR
336 and EGFR (Letizia et al., 2023; Olivares-Castineira and Llimargas, 2017), and were
337 identified in the surface proteome analysis. Consistently, knockdown of *rab5* or *rab7*
338 in fat body reduced the activity of JAK/STAT signaling in the progenitor cells (Figure
339 7D-F). Corroborating the genetic manipulations, BFA treatment that impeded
340 vesicular transport also resulted in impairment of JAK/STAT signaling in trachea
341 (Figure 7G-I). Taking advantage of the aforementioned DIPF reporter to assess the
342 response of receiving cells to ligands, we found that the fluorescent signal of DIPF
343 was compromised upon the presence of BFA, but was unaffected by inhibitors that
344 target the downstream JAK protein (Figure 7J-M), suggesting that signaling ligands
345 are less abundant in the recipient progenitor cells and that the vesicle-mediated
346 transport of ligands is essential for JAK/STAT signaling.
347 Phenotypically, the tracheal progenitors exhibited bidirectional migration in BFA-
348 treated flies, which phenocopies JAK/STAT loss-of-function (Figure 7N-P). In

349 concord with this observation, depletion of *grasp65* or *lbm* also led to bidirectional
350 movement (Figure 7Q-S'', and Video 6). Similar observations were made in tracheal
351 progenitors with either *rab5* or *rab7* knockdown (Figure 7T-V), whereas perturbation
352 of neither *rab2* nor *rab3* affected the disciplined progenitor migration (Figure 7-figure
353 supplement 1A-C). Taken together, these results suggest that JAK/STAT signaling in
354 the trachea is dependent on the vesicle-mediated transport of its ligands from fat body.
355
356 <u>The interaction between Upd2 and endocytic machinery</u>
357 Our results described thus far suggest that Upd2 emanating from fat body signals to
358 JAK/STAT signaling in the trachea. To further explore the molecular basis underlying
359 the vesicular transport of Upd2, we monitored Rab5-GFP and Rab7-GFP in fat body,
360 which mark early and late endosomes, respectively (Vonderheit and Helenius, 2005).
361 The fat body-produced Upd2 appeared vesicular (Figure 8A) and both Rab5 and Rab7
362 were found adjacent to the Upd2-harboring vesicles, suggesting that both Rab
363 GTPases function in the transport of Upd2 (Figure 8A'-B''). In contrast, Rab3
364 exhibited non-overlapping distribution with Upd2 (Figure 7-figure supplement 1E-
365 E''). Furthermore, we observed that Grasp65 was in close proximity to Upd2-
366 containing vesicles, indicating its integral roles in these vesicles (Figure 8C-C''). In
367 addition, Upd2 was observed to colocalize with the tetraspanin, Lbm (Figure 8D-D'').
368 At higher resolution, Upd2 and Lbm showed close association in a supramolecular
369 configuration (Figure 8D'''and 8D''''), corroborating its role in the transport of Upd2.
370 To determine if Upd2 interacts with the coordinators of vesicle trafficking, we
371 employed the Duolink in situ proximity ligation assay (PLA) which revealed strong
372 interactions between Upd2 and Rabs, such as Rab5 and Rab7 (Figure 8E-H), as well
373 as Lbm (Fig 8I, J). The interaction was further validated by the revelation that Upd2
374 co-immunoprecipitated with Rab5 and Rab7 (Figure 8K, L). The presence of Upd2 in
375 Lbm-containing vesicles was also evidenced in S2 cells (Figure 8-figure supplement
376 1A-C'') and co-IP experiment showed that Lbm physically associated with Upd2 in
377 both fat body and S2 cells (Figure 8M and Figure 8-figure supplement 1F). To further
378 understand the biogenesis of Lbm-containing vesicles that transport Upd2, we

379 conducted electron microscopic analysis of the Lbm-containing vesicles through the
380 expression of an HRP-fused Lbm in the fat body (Figure 8-figure supplement 1D).
381 The interaction between Lbm and Upd2 as simulated by Alphafold2 supported their
382 direct association (Figure 8-figure supplement 1E). Then, we generated an Lbm
383 chimera tagged with a pH-sensitive GFP variant, pHluorin (Yoshihara et al., 2005).
384 PHluorin fluorescence is squelched at the low pH domain such as in intravesicular
385 compartments, but becomes detectable when exposed to the extracellular
386 environment, thus enabling detection of exocytosis and endocytosis. Fat body
387 expressing Lbm-pHluorin produced GFP puncta at the plasma membrane (Figure 8N),
388 and the GFP signal was also detected in the trachea, suggesting the reception and
389 internalization of Lbm-containing vesicles by tracheal cells (Figure 8O). However, the
390 GFP fluorescence in both fat body and trachea was dramatically decreased by BFA
391 treatment, suggesting that Lbm-containing vesicles are diminished (Figure 8-figure
392 supplement 1G-J). Accordingly, the signals of Lbm-pHluorin in both fat body and
393 responding tracheoblasts were apparently compromised when Rab5 or Rab7 was
394 perturbed (Figure 8P-S), suggesting that the biogenesis and production of Lbm-
395 containing vesicles depend on Rab-mediated vesicle trafficking. Taken together, these
396 results suggest that fat body-derived Upd2 interacts with Rab-mediated endocytic
397 trafficking system to control the disciplined movement of tracheal progenitors.
398

Discussion

Resident stem cells and progenitors are mobilized to regenerate damaged or degenerated tissue. Despite the large distance between the niche where stem cells interact with their microenvironments and the destination for reconstruction, their commitment to a stereotyped track implicates sophisticated mechanism that controls disciplined migration as stem cells are activated and move out of the niche. While primary inducers expressed by damaged tissues are in play to coordinate the newly generated architecture with the degenerated counterpart (Chen and Krasnow, 2014), the present study elucidates an integral role of Upd2-JAK-STAT pathway in regulating the expression of polarity-related genes and maintaining the disciplined migration of tracheal progenitors (Figure 8T). The transport of Upd2 from fat body to trachea suggests intensive inter-organ communication during the migration of tracheal progenitors.

Several possibilities could account for the JAK/STAT-dependent polarity. The signaling components of JAK/STAT pathway could exhibit polarized localization (Sotillos et al., 2008). Alternatively, this signaling may activate genes controlling cell polarity and adhesion (Mallart et al., 2024; Tsurumi et al., 2011). Functional interplay between JAK/STAT signaling and cell polarity has been observed in various contexts (Chatterjee et al., 2023; Zeidler et al., 1999). Our results support a role of JAK/STAT signaling in promoting expression of genes with established roles in planar polarity, which may hallmark the route for the migration of the tracheal progenitor cells.

Epithelial cells exhibit two aspects of polarity: apical-basal polarity and planar cell polarity (PCP). The latter refers to the collective alignment of cell polarity within the plane of an epithelial sheet (Zallen, 2007). Molecularly, PCP is generated by the asymmetry of a group of proteins (PCP proteins) that mediate communication between neighboring cells (Barlan et al., 2017a; Matis and Axelrod, 2013; Williams et al., 2022). In *Drosophila*, the components of PCP are considered to group functionally into two core modules. The seven-pass transmembrane protein Frizzled (Fz), the cytosolic proteins Dishevelled (Dsh), Diego (Dgo), the four-pass transmembrane protein Strabismus (Stbm, also known as Van Gogh (Vang)) and the cytosolic protein

429 Prickle (Pk) belong to the first module. The second module consists of Fat (Ft; also
430 known as cadherin-related tumor suppressor), Dachsous (Ds), Four-jointed (Fj) and
431 Atro (a transcription repressor) (Peng and Axelrod, 2012). Intensive functional
432 interplay occurs between these two modules (Ayukawa et al., 2014). Aberrant activity
433 of the core PCP proteins leads to misoriented hairs and complex swirling patterns (Ma
434 et al., 2003; Wong and Adler, 1993). In addition to arrangement of epithelial
435 appendages, PCP pathway is also required for collective and directed cell movements
436 (Munoz-Soriano et al., 2012). The migratory cell cohort is polarized into 'pioneer'
437 cells that lead the trailing followers (Vitorino and Meyer, 2008).
438 Our data indicate that expression of Ds, Fj, Fz, Stan and Fat2, core components or
439 regulators of PCP, depends on JAK/STAT pathway. The interaction between atypical
440 cadherin Fat (Ft) and its ligand, Dachsous (Ds) directs core protein asymmetry (Strutt
441 and Strutt, 2021; Yang et al., 2002). Phenotypically, aberrancy of PCP protein
442 abundance, either excessive core protein or deficit in expression gradients, gives rise
443 to similar morphological abnormality (Adler et al., 2000; Casal et al., 2002; Taylor et
444 al., 1998; Tree et al., 2002). Consistent with this notion, gain-of-function of Fj or Ds
445 phenocopies that of perturbation of PCP proteins. JAK/STAT signaling promotes the
446 expression of Ds, but reduces Ft expression (Figure 4). Thereby, perturbation of
447 JAK/STAT signaling disrupts the Ds-Ft system.
448 A precedent for JAK/STAT signaling in directional cell movement is border cell
449 migration from anterior to posterior compartment during *Drosophila* oogenesis.
450 Migration of the border cells is guided by a gradient of PDGF and VEGF chemokines
451 (Duchek et al., 2001). Loss of either *hop* (encoding JAK) or *stat* in the border cells
452 impinges their recruitment into the cluster and subsequent migration (Silver et al.,
453 2005). Our results suggest that JAK/STAT signaling does not serve as a guidance cue
454 for tracheal progenitors, but rather directs the directionality of cell movement. The
455 downstream PCP components may contribute to either polarity of progenitors or cell-
456 cell interactions between the progenitors and tracheal cells that they track along. It
457 remains unknown how individual progenitor cells perceive directional information
458 and convert it into group choreography.

459 We identified the fly fat body as the major source for the JAK/STAT signaling ligand,
460 Upd2 production. Fat body is functionally equivalent to the mammalian liver which
461 stores proteins, lipids and sugars and functions as an energy reservoir (Li et al., 2019).
462 It supplies proteins and/or hormones that are utilized by other organs, and thereby
463 serves as an interchange center to disperse systemic hormonal and nutritional signals.
464 For instance, it generates collagen IV to decorate imaginal discs and produces
465 xanthine dehydrogenase for eye pigmentation (Pastor-Pareja and Xu, 2011; Reaume et
466 al., 1989). The transport between fat body and trachea has been reported on a secreted
467 chitin deacetylase, Serpentine (Serp), which is expressed by fat body and contributes
468 to tracheal morphogenesis (Dong et al., 2014). Our results reveal that fat body also
469 signals to regulate the disciplined migration of tracheal progenitors through the
470 dispersion of Upd2 cytokines. These studies collectively suggest that fat body
471 orchestrates systemic tissue growth and patterning and that metabolic regulation is
472 critical for adult stem cells.
473 Proteins that are locally produced can execute systemic function in distant organs. A
474 possible route of transport is through the hemolymph or bloodstream and taken up by
475 the target tissues. The signaling proteins such as cytokines can be packaged in
476 extracellular vesicles with various dimensions (Buzas, 2023; Javeed et al., 2021). A
477 precedent of vesicular transport of signaling molecules is reported in migrasomes
478 whose diameter exceeds 500 nm (Jiang et al., 2019).
479 These extracellular vesicles mediate cell-to-cell communication (Colombo et al.,
480 2014), perhaps at a distance (Hood et al., 2011) and even traverse between organs
481 (Corrigan et al., 2014). The vesicular Upd2 is able to signal at recipient cells,
482 suggesting that the activity of Upd2 is preserved in the vesicle, and it is released upon
483 vesicle fusion. Compared with conventional extracellular vesicles such as exosomes,
484 the Upd2-containing vesicles possess larger dimension. Its production and trafficking
485 depend on GRASP-mediated unconventional secretion and interaction with Lbm.
486 Lbm belongs to the tetraspanin protein family that contains four transmembrane
487 domains. The mammalian homologs of tetraspanins, CD9, CD63, CD81 or CD37 are
488 principal constituents of extracellular vesicles. The Lbm-containing vesicles are

regulated by GRASP-mediated secretion and are sensitive to pharmacological inhibition of EV transport.

It has been proposed that tetraspanins facilitate regeneration and wound healing in cultural cells and single-cell plasma membrane. Tetraspanin-enriched macrodomains are assembled into a ring-like structure (Huang et al., 2022), which is recruited to large membrane wounds and promotes membrane repair (Wang et al., 2022). The present study adds another dimension to the roles of tetraspanin proteins in tissue regeneration which can be ascribed to transport of signaling proteins and modulation of stem cells.

REAGENT or RESOURCE	SOURCE	IDENTIFIER
Antibodies		
Rabbit anti-GFP (1:400)	Invitrogen	#A11122
Mouse anti-GFP (1:1000)	Abclonal	#AE012
Mouse anti-mCherry (1:1000)	Abclonal	#AE002
Rabbit anti-tubulin (1:5000)	Baoke	#BK7010
Phalloidin Alexa Fluor 640 (1:50)	Biotum	#00050
HRP-conjugated Streptavidin (1:5000)	Proteintech	#SA00001-0
Alexa Fluor 488 (1:200)	Abclonal	#AS053
Alexa Fluor 555 (1:200)	Abclonal	#AS007
DAPI	VECTASHIELD	#H1200
Reagents		
Halocarbon oil 700	Sigma	#H8898
RNeasy Micro Kit	QIAGEN	#74004
SMART-Seq v4 Ultra low input RNA Kit	Takara	#634889
AMPure XP	Beckman Coulter	#A63882
TruePrep DNA Library Prep Kit V2	Vazyme	#TD501
Anti-FLAG M2 Magnetic Beads	Millipore	#8823
BXXP	APEXBIO	#A8012
Experimental models: Organisms/strains		
D. melanogaster:*UAS-upd2RNAi*	Tsinghua Stock Center	THU1331, THU1288
D. melanogaster:*UAS-domeRNAi*	Tsinghua Stock Center	THU0574, THU5825
D. melanogaster:*UAS-hopRNAi*	Tsinghua Stock Center	THU5762, TH201501042.S
D. melanogaster:UAS-stat92ERNAi	Tsinghua Stock Center	THU0573, THU1915
D. melanogaster:*UAS-lbmRNAi*	Tsinghua Stock Center	THU2602, BDSC27278
D. melanogaster:*UAS-grasp65RNAi*	Tsinghua Stock Center	TH04282.N, THU1429
D. melanogaster:*UAS-rab5RNAi*	Tsinghua Stock Center	TH02192.N, THU0671
D. melanogaster:*UAS-rab7RNAi*	Tsinghua Stock Center	TH02539.N, THU2437
D. melanogaster:UAS-fjRNAi	Tsinghua Stock Center	THU201500988.S, THU1538
D. melanogaster:*UAS-fat2RNAi*	Tsinghua Stock Center	THU4120, VDRC27113
D. melanogaster:*UAS-yurtRNAi*	Tsinghua Stock Center	THU1740, VDRC28674
D. melanogaster:UAS-crbRNAi	Tsinghua Stock Center	THU2783, THU5212
D. melanogaster:UAS-scbRNAi	Tsinghua Stock Center	THU3905, THU2707
D. melanogaster:UAS-dsRNAi	Tsinghua Stock Center	THU2846, VDRC36219
D. melanogaster:UAS-ftRNAi	Tsinghua Stock Center	TH201500989.S, VDRC9396
D. melanogaster:*10XStat92E-GFP*	Tsinghua Stock Center	THJ0273
D. melanogaster:*Stat92E-GFP*	BDSC	#38670
D. melanogaster:*UAS-grasp65-GFP*	BDSC	#8507
D. melanogaster:*Ds::GFP*	BDSC	#59425
D. melanogaster:*Yurt::GFP*	VDRC	#318067
D. melanogaster:*Crb::GFP*	VDRC	#318384
D. melanogaster:*Ft::GFP*	VDRC	#318477
D. melanogaster:*Fj::GFP*	VDRC	#318457
D. melanogaster:*UAS-dsRNAi*	VDRC	#36219
D. melanogaster:*UAS-ftRNAi*	VDRC	#9396
D. melanogaster:*UAS-ft*	(Brittle et al., 2010)	
D. melanogaster:*UAS-ds*	(Brittle et al., 2012)	
D. melanogaster: *fat2-GFP*	(Barlan et al., 2017b)	
D. melanogaster:*UAS-GFP-Rab7*	BDSC	#9779
D. melanogaster:*UAS-GFP-Rab5*	BDSC	#24616
D. melanogaster:hop^{Tum}/*FM7C*	BDSC	#8492
D. melanogaster:$stat92E^{F}$	BDSC	#24757
D. melanogaster:$dome^{G0264}$	Kyoto	#111866

Oligonucleotides

Materials and methods

Primer α-tubulin84b Forward:CACACCACCCTGGAGCATTC	This paper	N/A
Primer α-tubulin84b Reverse:CCAATCAGACGGTTCAGGTTG	This paper	N/A
Primer upd2 Forward:TCAATCCGTATCGCGGTCTG	This paper	N/A
Primer upd2 Reverse:AGAAGAGTCGCAGGTTGTGG	This paper	N/A
Primer ds Forward:ACAACCGAACTCGAACCGAA	This paper	N/A
Primer ds Reverse:AGTAGCATCACACACAAGTGA	This paper	N/A
Primer ft Forward:CTGGATCGAGAGCAGCAGAG	This paper	N/A
Primer ft Reverse:GACGGTAAATTCTCGCGCAC	This paper	N/A
Primer fj Forward:ATTACTCAAGCGGTTGGGGG	This paper	N/A
Primer fj Reverse:CGGTTCCTGTTCCTGTCTCC	This paper	N/A
Primer fat2 Forward:TATCTGCGCCCATACGCATT	This paper	N/A
Primer fat2 Reverse:TCTCATCGGCCTTGCTTTGT	This paper	N/A
Primer yurt Forward:GGTCAGCTCAGGGTGACTATC	This paper	N/A
Primer yurt Reverse:ATTGGTAAGCTTGGCGTTGC	This paper	N/A
Primer crb Forward:CAGCAGTGTTTGAACGGTGG	This paper	N/A
Primer crb Reverse:AGGCAGTGACCAATGGGG	This paper	N/A
Software and algorithms		
Fiji / ImageJ	NIH	RRID:SCR_002285
GraphPad Prism 8.0	GraphPad Software	https://www.graphpad.com/scientific-software/prism/
Zen 3.1	Zeiss	https://www.zeiss.com.cn/corporate/home.html
PCA-flow	Bradski, G.[79]	https://www.drdobbs.com/open-source/the-opencv-library
Deposited data		
Raw and processing Data	This paper	GSE256177 https://www.iprox.cn/page/PSV023.html;?url=1708323921277ZyfCqvupguyijvyndyf

Key Resources Table

505

506 **Fly lines and husbandry**

507 All flies were reared on normal cornmeal and agar medium at 25℃ unless noted.
508 UAS-upd2RNAi (THU1331, THU1288), UAS-domeRNAi (THU0574), UAS-
509 hopRNAi (THU5762), UAS-stat92ERNAi (THU0573), UAS-lbmRNAi (THU2602),
510 UAS-grasp65RNAi (TH04282.N), UAS-rab5RNAi (TH02192.N), UAS-rab7RNAi
511 (TH02539.N), UAS-fjRNAi (THU201500988.S), UAS-fat2RNAi (THU4120), UAS-
512 yurtRNAi (THU1740), UAS-crbRNAi (THU2783) and UAS-scbRNAi (THU3905)
513 were ordered from Tsinghua Stock Center. Stat92E-GFP (BSDC#38670), UAS-
514 grasp65-GFP (BSDC#8507), Ds::GFP (BSDC#59425) were from Bloomington
515 Drosophila Stock Center. Yurt::GFP (v318067), Crb::GFP (v318384), Ft::GFP
516 (v318477), Fj::GFP (v318457), UAS-dsRNAi (v36219, THU2846), and UAS-ftRNAi
517 (v9396) were obtained from VDRC. UAS-ft was kindly provided by Dr. Xianjue Ma,
518 UAS-ds was kindly provided by Dr. Xing Wang and UAS-fat2-GFP was from Dr.
519 Shunfan Wu. UAS-GFP-rab5 and UAS-GFP-rab7 were kindly provided by Dr.
520 Xiaohang Yang.

521 **Plasmid construction and transgenic flies**

522 To generate UAS-upd2-mCherry and UAS-lbm-GFP, UAS-lbm-HRP transgenic flies,
523 the coding sequence of upd2 or lbm was PCR amplified from a fly cDNA library and
524 cloned into a pUAST vector with C-terminal mCherry, GFP or HRP.

525 The DIPF reporter was generated by first fusing cpYFP and *Drosophila* FKBP12 and
526 subsequently ligating to the dome cDNA via a GTG linker. The above product was
527 then cloned into a pUAST vector and verified by DNA sequencing, and injected into
528 y[1] M{vasint.Dm}ZH-2A w[*]; P{CaryP}attP2 recipient flies or *w1118* following
529 standard *Drosophila* transformation injection procedures (Core Facility of Drosophila
530 Resource and Technology, SIBCB, CAS).

531 **Cell culture and transfection**

532 S2 cells were grown in Schneider Drosophila Medium (Gibco, #21720024)
533 supplemented with 10% (v/v) Fetal Bovine Serum (FBS, Gibco, #10099141C) and
534 1% (v/v) Penicillin Streptomycin (Pen/Strep, Life Technologies) at 28°C with 0.2%
535 CO_2. Transfection was conducted with 5 μg plasmids (act-GAL4, UAS-lbm-GFP,
536 UAS-upd2-mCherry) using Effectene Transfection Reagent (QIAGEN, #301425).

537 SKOV3 cells were cultured in DMEM medium (CR#12800) containing 10% FBS
538 (Gibco, #10099141C) in an incubator with 5% CO2 at 37 °C. Cells with ~80%
539 confluency were infected with lentivirus loaded with siRNAs for gene knockdown or
540 gRNAs for knockout, and the medium was replaced 24 hours post-infection. 72 hours
541 after lentivirus infection, bright-field images were taken every 5 minutes for 12 hours
542 using a confocal microscope.

543 **Quantitative reverse transcription PCR**

544 Larval or pupal trachea were dissected in cold PBS, and then transferred to RNA
545 extraction reagent (AG21101). Next, reverse transcription was performed using qPCR
546 RT Mix with gDNA Remover reagent (AG11706). qPCR was performed using the
547 Universal SYBR Select Master Mix (AG11701) with a Bio-Rad system. The
548 foldchange of target gene expression was normalized to that of α-tubulin. The primers
549 are listed in Key Resources Table.

550 **Western Blotting and Co-immunoprecipitation**

551 Total protein was extracted from cells or tissues by RIPA buffer supplemented with a
552 protease inhibitor cocktail (Merck, #11836170001) and phenylmethanesulfonyl
553 fluoride (Beyotime, #ST507), separated by 10% SDS-PAGE gels and transferred to
554 PVDF membrane (Millipore, #IPVH00010). Blots were detected with an ECL
555 Western Blotting detection system (Bio-Rad). For co-immunoprecipitation, lysates of
556 larval fat body or transfected S2 cells were incubated overnight at 4°C with protein A
557 Magnetic beads (Thermo Scientific, #2736141) pre-coated with GFP antibody
558 (Invitrogen, #A11122). Immunoprecipitates were eluted in SDS-containing loading

559 buffer for subsequent immunoblotting analysis. Antibodies for immunoblotting
560 include: α-tubulin (Baoke, #BK7010), α-HRP-conjugated Streptavidin (Proteintech,
561 #SA00001-0), α-GFP (Abclonal, #AE012, 1:1000); α-mCherry (Abclonal, #AE002,
562 1:1000).

563 **Proximity Ligation Assay**

564 Proximity ligation assay (PLA) was carried out with Duolink® In Situ Detection
565 Reagents Far Red (Sigma Aldrich, #DUO92013) according to manufacturer's
566 instructions, using the probes anti-rabbit PLUS (Sigma Aldrich, #DUO92002) and
567 anti-mouse MINUS (Sigma Aldrich, #DUO92004). Briefly, larval fat body was
568 dissected and fixed in 4% formaldehyde. The animals not expressing upd2-mCherry
569 served as controls. After permeabilization, the samples were incubated with primary
570 antibodies overnight at 4°C. Then, the samples were washed with PLA buffer A,
571 hybridized with PLA probes, ligated, and amplified. Samples were washed twice with
572 PLA buffer B (Sigma Aldrich, #DUO82049) and fluorescence images were taken with
573 an LSM Zeiss 900 inverted confocal laser scanner microscope.

574 **Immunofluorescence**

575 Trachea from white pupae (0hr APF) were dissected in PBS and fixed with 4%
576 formaldehyde for 25 min at room temperature. After washes, trachea samples were
577 permeabilized with 1% TritonX-100 in PBS, and then blocked in 10% goat serum.
578 Incubation with primary antibody (GFP, 1:400; lacZ, 1:40) was performed at 4°C with
579 gentle rotation for overnight. Then, the samples were incubated with secondary
580 antibodies conjugated to Alexa Fluor 488 or 555 (1:200) and Phalloidin (1:50) for 2
581 hrs. After washing, samples were mounted in antifade mounting medium with DAPI
582 (VECTASHIELD) and imaged under an LSM Zeiss 900 inverted confocal laser
583 scanner microscope.

584 **Live imaging of pupal trachea stem cells**

585 White pupae (0hr APF) were briefly washed in double distilled water and mounted in

586 halocarbon oil 700 (Sigma, #H8898). The pupae were positioned with forceps to bring
587 a single dorsal trunk of the trachea up for optimal imaging of Tr4 and Tr5 metameres.
588 Then, pupae were immobilized by a 22x30 mm No.1.5 high precision coverslip
589 spaced by vacuum grease. Time-lapse images were captured by an LSM Zeiss 900
590 inverted confocal laser scanner microscope. For migration distance measurement, we
591 took sequential snapshots of the moving progenitors of pupae staged at 0hr, 1hr, 2hr
592 and 3hr APF. The migration distance was measured as the distance from the starting
593 position (the junction of TC and DT) to the leading edge of progenitor groups. The
594 migration velocity was calculated by v=d (micrometer)/t (min).

595 **RNA sequencing of tracheal progenitors**

596 Total RNA was isolated from the Tr4 and Tr5 metamere progenitors dissected from
597 1hr APF pupae using RNeasy Micro Kit (QIAGEN, #74004). SMART-Seq v4 Ultra
598 low input RNA Kit (Takara, #634889) was used for first-strand and second-strand
599 cDNA synthesis and double-stranded cDNA end repair. Double-stranded cDNAs were
600 cleaned using AMPure XP (Beckman Coulter, #A63882). Then cDNAs were
601 subjected to tagmentation and ligation to adaptors to generate the sequencing libraries
602 using TruePrep DNA Library Prep Kit V2 for Illumina kit (Vazyme, #TD501). The
603 quality and concentration of the libraries were assessed using the Agilent High
604 Sensitivity DNA Kit and Bioanalyzer 2100 (Agilent Technologies) and submitted to
605 150 bp paired-end high throughput sequencing using Hiseq4000 (Illumina).

606 Analysis of RNA-seq data was performed using a computer system equipped with
607 multiple processors. Clean reads were mapped to the *Drosophila* genome sequence
608 using Hisat2 with default parameters. Successfully mapped reads were counted using
609 FeatureCounts. Differential gene expression analysis was performed using the
610 DESeq2 package. Adjusted p-value < 0.05 was used as the threshold to identify the
611 differentially expressed genes. Gene ontology and KEGG pathway enrichment
612 analyses for the differentially expressed genes were conducted using the Database for
613 Annotation, Visualization and Integrated Discovery (DAVID).

614 **Chromatin Immunoprecipitation**

615 Third instar larval trachea from Stat92E-Flag (BDSC, #38670) were fixed in 1%
616 formaldehyde. The fixation reaction was terminated by adding glycine (125 mM).
617 Trachea were washed and resuspended in lysis buffer, and sonicated to generate 200-
618 600 bp DNA fragments. Procedures of immunoprecipitation and ChIP sequencing
619 library construction were as previously described (Li et al., 2022). Anti-FLAG M2
620 Magnetic Beads (Millipore, #8823) were used for enriched DNA binding to
621 transcription factor Stat92E.

622 Immunoprecipitated DNA was subjected to next-generation sequencing using the
623 Epicenter Nextera DNA Sample Preparation Kit or to real-time PCR. Library
624 construction was performed using the High Molecular Weight tagmentation buffer
625 (source), and tagmented DNA was linearly amplified by PCR. The libraries were then
626 sequenced on a Novaseq according to manufacturer's standard protocols. The
627 sequences were processed using *Fastqc* and low-quality bases and adaptor
628 contamination were trimmed by *cutadapt*. Filtered reads were mapped to *Drosophila*
629 genome using *BWA mem* algorithm. Peaks were called using macs2 *callpeak* (Zhao et
630 al., 2019) and plotted using pyGenomeTracks. GO analysis of biological processes
631 was conducted by DAVID.

632 **Cell-surface proteomics of fly trachea**

633 Trachea from white pupae were dissected in pre-cooled Schneider Medium (Gibco)
634 and collected in 1.5 mL low-binding tube (Axygen) containing 500 μL Schneider
635 Medium. The samples were washed with 500 μL fresh medium and incubated with
636 100 μM BXXP (APEXBIO, #A8012) for 1 hr on ice with occasional pipetting.
637 Labeling reaction was initiated by adding 1 mM (0.03%) H_2O_2 to the sample-
638 containing medium and proceeded for 7 minutes at room temperature. The reaction
639 was immediately quenched by five thorough washes with PBS containing 10 mM
640 sodium ascorbate (Aladdin, #S105024) and 5 mM Trolox (APEXBIO, #C3183). For
641 biochemical characterization or proteomic sample preparation, the quenching solution

642 was drained, and the trachea in minimal residual quenching solution were quickly
643 frozen in liquid nitrogen and stored at 80°C. LC-MS/MS analysis was performed
644 using a Q Exactive HF-X instrument (Thermo Fisher) coupled with Easy-nLC 1200
645 system. The acquired MS raw data were processed using MaxQuant version 2.0.1.0
646 (Max Planck Institute of Biochemistry, Germany). Label-free quantification (LFQ)
647 was set with a default parameter and iBAQ was selected.

648 **Transmission electron microscopy**

649 Fat body of third instar larvae were dissected and fixed in 0.12 M Na-cacodylate
650 buffer (pH 7.4) containing 2.5% glutaraldehyde for 1 hr on ice. Then the samples
651 were rinsed in 0.12 M Na-cacodylate buffer (6 × 5 min, on ice). The dissected fat
652 body were pre-incubated with DAB (10 mg/20 ml) in 0.12 M Na-cacodylate buffer
653 (containing 0.1% saponin) for 30 minutes with agitation in the dark. Then 30% H_2O_2
654 was quickly mixed in DAB solution to a 0.03% v/v concentration and reacted for 30
655 min at RT. The fat body were transferred to 0.12 M Na-cacodylate buffer (6 × 5 min,
656 RT). To increase the electron density of the HRP/DAB product, samples were
657 transferred into 0.01% OsO4 in 0.12 M Na-cacodylate buffer (pH 7.4) for 10 min at
658 RT, then rinsed in 0.12 M Na-cacodylate buffer (3 × 10 min, on ice). 0.1%
659 thiocarbohydrazide in 0.12 M Na-cacodylate buffer (pH 7.4) was used for 10 min at
660 RT, then rinsed in 0.12 M Na-cacodylate buffer (3 × 10 min, on ice). After post-
661 fixation for 1 hour at RT with 1% OsO4 in 0.12 M Na-cacodylate buffer (pH 7.4), the
662 samples were rinsed with MilliQ water (3 × 5 min, RT) and dehydrated in a series of
663 15 min with 10%, 30%, 50%, 70%, 90% and 100% (3×) ethanol. Infiltration was
664 conducted at RT with a mixture of acetone and resin 1:1 for 1.5 h, 1:2 for 3 h and 1:3
665 overnight. The tissues were then dissected from the carcasses and placed in block
666 molds filled with resin for hardening at 60°C during 48 h. 70 nm ultrathin section
667 from the hardened blocks were cut on a Leica EM UC7 ultramicrotome using an Ultra

45° diamond knife and imaged in a thermos scientific Talos L120C electron microscope.

Numeration of tracheal progenitors

The pupae at indicated stages were dissected and then fixed with 4% PFA for 25 minutes. The nuclei were labeled by DAPI. The samples were imaged by an LSM Zeiss 900 inverted confocal laser scanner microscope. The number of progenitor cells was scored from image stacks.

Optic Flow Analysis

Motion Correlation

Time-lapse images of trachea progenitor cells were captured every 5 minutes over a total duration of 2 hrs using an LSM Zeiss 900 microscope. The movies and images were subjected to a three-step motion collection using ImageJ (Schneider et al., 2012) as follows:

(1) Images were transformed to grey scale.

(2) Automated stabilization was performed on grey images by image stabilizer.

(3) The feature points were mapped and affine transformation was applied using big warp (Bogovic et al., 2015).

Optical flow

Optical flow represents the pattern of motion of pixels in a sequence of images. Between two consecutive frames $I(x, y, t)$ and $I(x, y, t + \Delta t)$, the optical flow vector $\mathbf{v} = (v_x, v_y)$ represents the motion of pixels during this time. The optical flow constraint equation is shown below:

$$I_x v_x + I_y v_y + I_t = 0$$

We adopted the PCA-flow algorithm (Bradski, 2000) in openCV library (cv::optflow::OpticalFlowPCAFlow) in which the sparse optical flow vectors within each small region of the image sequence are calculated before training optical flow fields via principal component analysis (PCA) (Wulff and Black, 2015). The vectors were assembled to generate a smooth vector field of optic flow using the learning linear models of flow. The PCA-flow was validated for the efficiency and robustness.

Variance in 1D axis

We developed a robust estimator to evaluate the variance of optic flow projection along the 1D migration axis between samples. The vector length is normalized by a frame-specific normalization factor κ to fit with scale of optic flow computed among different frames.

$$\kappa = Q_{0.9}\{||v||_2 \mid v \in vectorfield\}$$

where Q is the quantile function. The variance is computed as $\mathrm{Var}(\{||v||_2 > Q_{0.2} \mid v \in vectorfield\})$ and scaled to 0-1 by $\mathrm{Var}(x)/\big(\mathrm{Var}(x) + \mathrm{Var}(y)\big)$.

Random Variable

The direction of optic flow in each volume was assigned to ’left’ or ’right’. Then the distribution of the binarized directions is modeled as a Bernoulli random variable $\mathrm{X} \sim \mathrm{Bernoulli(p)}$ with PMF

$$P(X = x) = \begin{cases} p & \text{if } x = 1, \\ 1 - p & \text{if } x = 0. \end{cases}$$

Binary Entropy

The entropy for Bernoulli random variable $\mathrm{X} \sim \mathrm{Bernoulli(p)}$ is defined as

$$H_{binary}(X) = -p\log(p) - (1-p)log(1-p)$$

The entropy evaluates the information contained in the random variable (also called uncertainty). In this case, when $p = 0.5$, it reaches the maxima 1; if the variable is determinate (i.e. p=0 or 1), the entropy is zero. More directed cell migration leads to a lower entropy in optic flow since the certainty is high for the migration direction. We estimated p by computing ratio of left and right direction

$$p = \frac{\#left}{\#left + \#right}$$

Image and statistical analysis

Confocal z-stack images were analyzed to extract information of fluorescent intensity of stat92E-GFP and DIPF, and the number of Upd2-mCherry-containing vesicles. z slices of fluorescent intensity for Ds, Ft and Fj were measured. The number of particles for DIPF and Upd2-mCherry-containing vesicles was analyzed using ImageJ. All statistical analysis was conducted using GraphPad Prism 8.0. Mean and standard error of the mean (SEM) were shown. Unpaired *t*-tests with Benjamin's correction were used to evaluate statistical significance between groups.

Acknowledgements

We thank Drs Thomas Kornberg, David Strutt, Xiaohang Yang, Markus Affolter, Mark Krasnow, Stefan Luschnig, Kai Yuan, Xing Wang, Zhouhua Li, Xianjue Ma, Sarah Bray, Yiming Zheng and Shunfan Wu for generously providing reagents; Core Facility of Drosophila Resource and Technology, SIBCB, CAS for injection service; Bloomington Drosophila Stock Center, Kyoto Stock Center, Vienna stock center, Tsinghua Stock Center for fly stocks; Developmental Studies Hybridoma Bank for antibodies; all members of Huang lab and Kornberg lab for discussions and constructive suggestions. This work has been financially supported by NSFC92168101, NSFC32070784 and Thousand Young Talent Program to H.H., NSFC32000574 to H.G.W., National Key R&D Program of China (2022YFF0608402) and Chinese National Natural Science Funds (22374128) to B.Y. and NSFC32300699, LQ24C120001 and Postdoctoral Fellowship Foundation 2023M733098 to Y.L..

Author contributions

Conceptualization: H.H., P.Z.D.; Methodology: B.Y., P.Z.D., T.F.L., T.Y.G; Investigation: P.Z.D., Y.L., Y.Y.W., Q.Z., T.F.L., H.G.W; Supervision: J.M., H.H., H.G.W, B.Y.; Writing: J.M., H.H., P.Z.D, H.G.W.

Declaration of interests

The authors declare no competing interests.

745 **References**

746

747 Adler, P.N., Taylor, J., and Charlton, J. (2000). The domineering non-autonomy of frizzled and van
748 Gogh clones in the Drosophila wing is a consequence of a disruption in local signaling. Mech Dev *96*,
749 197-207.
750 Agaisse, H., Petersen, U.M., Boutros, M., Mathey-Prevot, B., and Perrimon, N. (2003). Signaling role
751 of hemocytes in Drosophila JAK/STAT-dependent response to septic injury. Dev Cell *5*, 441-450.
752 Ambegaonkar, A.A., Pan, G., Mani, M., Feng, Y., and Irvine, K.D. (2012). Propagation of Dachsous-
753 Fat planar cell polarity. Curr Biol *22*, 1302-1308.
754 Andreu, Z., and Yanez-Mo, M. (2014). Tetraspanins in extracellular vesicle formation and function.
755 Front Immunol *5*, 442.
756 Arbouzova, N.I., and Zeidler, M.P. (2006). JAK/STAT signalling in Drosophila: insights into conserved
757 regulatory and cellular functions. Development *133*, 2605-2616.
758 Ayukawa, T., Akiyama, M., Mummery-Widmer, J.L., Stoeger, T., Sasaki, J., Knoblich, J.A., Senoo, H.,
759 Sasaki, T., and Yamazaki, M. (2014). Dachsous-dependent asymmetric localization of spiny-legs
760 determines planar cell polarity orientation in Drosophila. Cell Rep *8*, 610-621.
761 Bach, E.A., Ekas, L.A., Ayala-Camargo, A., Flaherty, M.S., Lee, H., Perrimon, N., and Baeg, G.H.
762 (2007). GFP reporters detect the activation of the Drosophila JAK/STAT pathway in vivo. Gene Expr
763 Patterns *7*, 323-331.
764 Barlan, K., Cetera, M., and Horne-Badovinac, S. (2017a). Fat2 and Lar Define a Basally Localized
765 Planar Signaling System Controlling Collective Cell Migration. Dev Cell *40*, 467-477 e465.
766 Barlan, K., Cetera, M., and Horne-Badovinac, S. (2017b). Fat2 and Lar Define a Basally Localized
767 Planar Signaling System Controlling Collective Cell Migration. Dev Cell *40*, 467-477.e465.
768 Beshel, J., Dubnau, J., and Zhong, Y. (2017). A Leptin Analog Locally Produced in the Brain Acts via a
769 Conserved Neural Circuit to Modulate Obesity-Linked Behaviors in Drosophila. Cell Metab *25*, 208-
770 217.
771 Bogovic, J.A., Hanslovsky, P., Wong, A., and Saalfeld, S. (2015). Robust registration of calcium images
772 by learned contrast synthesis. 2016 IEEE 13th International Symposium on Biomedical Imaging
773 (ISBI), 1123-1126.
774 Bradski, G. (2000). The OpenCV library. Dr Dobb's J Software Tools *25*, 120-125.
775 Brittle, A., Thomas, C., and Strutt, D. (2012). Planar Polarity Specification through Asymmetric
776 Subcellular Localization of Fat and Dachsous. Current Biology *22*, 907-914.
777 Brittle, A.L., Repiso, A., Casal, J., Lawrence, P.A., and Strutt, D. (2010). Four-jointed modulates
778 growth and planar polarity by reducing the affinity of dachsous for fat. Curr Biol *20*, 803-810.
779 Buzas, E.I. (2023). The roles of extracellular vesicles in the immune system. Nat Rev Immunol *23*,
780 236-250.
781 Casal, J., Struhl, G., and Lawrence, P.A. (2002). Developmental compartments and planar polarity in
782 Drosophila. Curr Biol *12*, 1189-1198.
783 Cetera, M., Ramirez-San Juan, G.R., Oakes, P.W., Lewellyn, L., Fairchild, M.J., Tanentzapf, G.,
784 Gardel, M.L., and Horne-Badovinac, S. (2014). Epithelial rotation promotes the global alignment of
785 contractile actin bundles during Drosophila egg chamber elongation. Nat Commun *5*, 5511.
786 Chakrabarti, S., Dudzic, J.P., Li, X., Collas, E.J., Boquete, J.P., and Lemaitre, B. (2016). Remote
787 Control of Intestinal Stem Cell Activity by Haemocytes in Drosophila. PLoS Genet *12*, e1006089.
788 Chatterjee, D., Cong, F., Wang, X.F., Machado Costa, C.A., Huang, Y.C., and Deng, W.M. (2023). Cell

789 polarity opposes Jak/STAT-mediated Escargot activation that drives intratumor heterogeneity in a
790 Drosophila tumor model. Cell Rep *42*, 112061.
791 Chen, F., and Krasnow, M.A. (2014). Progenitor outgrowth from the niche in Drosophila trachea is
792 guided by FGF from decaying branches. Science *343*, 186-189.
793 Chen, H.W., Chen, X., Oh, S.W., Marinissen, M.J., Gutkind, J.S., and Hou, S.X. (2002). mom identifies
794 a receptor for the Drosophila JAK/STAT signal transduction pathway and encodes a protein distantly
795 related to the mammalian cytokine receptor family. Genes Dev *16*, 388-398.
796 Cherbas, L., Hu, X., Zhimulev, I., Belyaeva, E., and Cherbas, P. (2003). EcR isoforms in Drosophila:
797 testing tissue-specific requirements by targeted blockade and rescue. Development *130*, 271-284.
798 Cho, E., and Irvine, K.D. (2004). Action of fat, four-jointed, dachsous and dachs in distal-to-proximal
799 wing signaling. Development *131*, 4489-4500.
800 Colombo, M., Raposo, G., and Thery, C. (2014). Biogenesis, secretion, and intercellular interactions of
801 exosomes and other extracellular vesicles. Annu Rev Cell Dev Biol *30*, 255-289.
802 Corrigan, L., Redhai, S., Leiblich, A., Fan, S.J., Perera, S.M., Patel, R., Gandy, C., Wainwright, S.M.,
803 Morris, J.F., Hamdy, F.*, et al.* (2014). BMP-regulated exosomes from Drosophila male reproductive
804 glands reprogram female behavior. J Cell Biol *206*, 671-688.
805 Darnell, J.E., Jr. (1997). STATs and gene regulation. Science *277*, 1630-1635.
806 Dong, B., Miao, G., and Hayashi, S. (2014). A fat body-derived apical extracellular matrix enzyme is
807 transported to the tracheal lumen and is required for tube morphogenesis in Drosophila. Development
808 *141*, 4104-4109.
809 Duchek, P., Somogyi, K., Jekely, G., Beccari, S., and Rorth, P. (2001). Guidance of cell migration by
810 the Drosophila PDGF/VEGF receptor. Cell *107*, 17-26.
811 Ertekin, D., Kirszenblat, L., Faville, R., and van Swinderen, B. (2020). Down-regulation of a cytokine
812 secreted from peripheral fat bodies improves visual attention while reducing sleep in Drosophila. PLoS
813 Biol *18*, e3000548.
814 Fuchs, E., and Blau, H.M. (2020). Tissue Stem Cells: Architects of Their Niches. Cell Stem Cell *27*,
815 532-556.
816 Heinrich, P.C., Behrmann, I., Haan, S., Hermanns, H.M., Muller-Newen, G., and Schaper, F. (2003).
817 Principles of interleukin (IL)-6-type cytokine signalling and its regulation. Biochem J *374*, 1-20.
818 Hombria, J.C., Brown, S., Hader, S., and Zeidler, M.P. (2005). Characterisation of Upd2, a Drosophila
819 JAK/STAT pathway ligand. Dev Biol *288*, 420-433.
820 Hood, J.L., San, R.S., and Wickline, S.A. (2011). Exosomes released by melanoma cells prepare
821 sentinel lymph nodes for tumor metastasis. Cancer Res *71*, 3792-3801.
822 Huang, Y., Zhang, X., Wang, H.W., and Yu, L. (2022). Assembly of Tetraspanin-enriched
823 macrodomains contains membrane damage to facilitate repair. Nat Cell Biol *24*, 825-832.
824 Ingaramo, M.C., Sanchez, J.A., Perrimon, N., and Dekanty, A. (2020). Fat Body p53 Regulates
825 Systemic Insulin Signaling and Autophagy under Nutrient Stress via Drosophila Upd2 Repression. Cell
826 Rep *33*, 108321.
827 Javeed, N., Her, T.K., Brown, M.R., Vanderboom, P., Rakshit, K., Egan, A.M., Vella, A., Lanza, I., and
828 Matveyenko, A.V. (2021). Pro-inflammatory beta cell small extracellular vesicles induce beta cell
829 failure through activation of the CXCL10/CXCR3 axis in diabetes. Cell Rep *36*, 109613.
830 Jiang, D., Jiang, Z., Lu, D., Wang, X., Liang, H., Zhang, J., Meng, Y., Li, Y., Wu, D., Huang, Y.*, et al.*
831 (2019). Migrasomes provide regional cues for organ morphogenesis during zebrafish gastrulation. Nat
832 Cell Biol *21*, 966-977.

Jones, D.L., and Wagers, A.J. (2008). No place like home: anatomy and function of the stem cell niche. Nat Rev Mol Cell Biol *9*, 11-21.

Kandere-Grzybowska, K., Letourneau, R., Kempuraj, D., Donelan, J., Poplawski, S., Boucher, W., Athanassiou, A., and Theoharides, T.C. (2003). IL-1 induces vesicular secretion of IL-6 without degranulation from human mast cells. J Immunol *171*, 4830-4836.

Krautz, R., Khalili, D., and Theopold, U. (2020). Tissue-autonomous immune response regulates stress signaling during hypertrophy. eLife *9*, e64919.

Laprise, P., Beronja, S., Silva-Gagliardi, N.F., Pellikka, M., Jensen, A.M., McGlade, C.J., and Tepass, U. (2006). The FERM protein Yurt is a negative regulatory component of the Crumbs complex that controls epithelial polarity and apical membrane size. Dev Cell *11*, 363-374.

Letizia, A., Espinas, M.L., Giannios, P., and Llimargas, M. (2023). The TNFR Wengen regulates the FGF pathway by an unconventional mechanism. Nat Commun *14*, 5874.

Li, J., Han, S., Li, H., Udeshi, N.D., Svinkina, T., Mani, D.R., Xu, C., Guajardo, R., Xie, Q., Li, T.*, et al.* (2020). Cell-Surface Proteomic Profiling in the Fly Brain Uncovers Wiring Regulators. Cell *180*, 373-386 e315.

Li, L., and Clevers, H. (2010). Coexistence of quiescent and active adult stem cells in mammals. Science *327*, 542-545.

Li, S., Yu, X., and Feng, Q. (2019). Fat Body Biology in the Last Decade. Annu Rev Entomol *64*, 315-333.

Li, Y., Dong, P., Yang, Y., Guo, T., Zhao, Q., Miao, D., Li, H., Lu, T., Xia, F., Lyu, J.*, et al.* (2022). Metabolic control of progenitor cell propagation during Drosophila tracheal remodeling. Nat Commun *13*, 2817.

Ma, D., Yang, C.H., McNeill, H., Simon, M.A., and Axelrod, J.D. (2003). Fidelity in planar cell polarity signalling. Nature *421*, 543-547.

Ma, J., Chen, T., Wu, S., Yang, C., Bai, M., Shu, K., Li, K., Zhang, G., Jin, Z., He, F.*, et al.* (2019). iProX: an integrated proteome resource. Nucleic Acids Res *47*, D1211-D1217.

Mallart, C., Netter, S., Chalvet, F., Claret, S., Guichet, A., Montagne, J., Pret, A.M., and Malartre, M. (2024). JAK-STAT-dependent contact between follicle cells and the oocyte controls Drosophila anterior-posterior polarity and germline development. Nat Commun *15*, 1627.

Matakatsu, H., and Blair, S.S. (2004). Interactions between Fat and Dachsous and the regulation of planar cell polarity in the
wing. Development *131*, 3785-3794.

Matis, M., and Axelrod, J.D. (2013). Regulation of PCP by the Fat signaling pathway. Genes Dev *27*, 2207-2220.

Michel, M., Raabe, I., Kupinski, A.P., Perez-Palencia, R., and Bokel, C. (2011). Local BMP receptor activation at adherens junctions in the Drosophila germline stem cell niche. Nat Commun *2*, 415.

Munoz-Soriano, V., Belacortu, Y., and Paricio, N. (2012). Planar cell polarity signaling in collective cell movements during morphogenesis and disease. Curr Genomics *13*, 609-622.

O'Shea, J.J., Gadina, M., and Schreiber, R.D. (2002). Cytokine signaling in 2002: new surprises in the Jak/Stat pathway. Cell *109 Suppl*, S121-131.

Olivares-Castineira, I., and Llimargas, M. (2017). EGFR controls Drosophila tracheal tube elongation by intracellular trafficking regulation. PLoS Genet *13*, e1006882.

Palmroth, M., Kuuliala, K., Peltomaa, R., Virtanen, A., Kuuliala, A., Kurttila, A., Kinnunen, A., Leirisalo-Repo, M., Silvennoinen, O., and Isomaki, P. (2021). Tofacitinib Suppresses Several JAK-

STAT Pathways in Rheumatoid Arthritis In Vivo and Baseline Signaling Profile Associates With Treatment Response. Front Immunol *12*, 738481.

Pastor-Pareja, J.C., and Xu, T. (2011). Shaping cells and organs in Drosophila by opposing roles of fat body-secreted Collagen IV and perlecan. Dev Cell *21*, 245-256.

Peng, Y., and Axelrod, J.D. (2012). Asymmetric protein localization in planar cell polarity: mechanisms, puzzles, and challenges. Curr Top Dev Biol *101*, 33-53.

Perochon, J., Yu, Y., Aughey, G.N., Medina, A.B., Southall, T.D., and Cordero, J.B. (2021). Dynamic adult tracheal plasticity drives stem cell adaptation to changes in intestinal homeostasis in Drosophila. Nat Cell Biol *23*, 485-496.

Pitsouli, C., and Perrimon, N. (2010). Embryonic multipotent progenitors remodel the Drosophila airways during metamorphosis. Development *137*, 3615-3624.

Rajan, A., Housden, B.E., Wirtz-Peitz, F., Holderbaum, L., and Perrimon, N. (2017). A Mechanism Coupling Systemic Energy Sensing to Adipokine Secretion. Dev Cell *43*, 83-98 e86.

Rajan, A., and Perrimon, N. (2012). Drosophila cytokine unpaired 2 regulates physiological homeostasis by remotely controlling insulin secretion. Cell *151*, 123-137.

Reaume, A.G., Clark, S.H., and Chovnick, A. (1989). Xanthine dehydrogenase is transported to the Drosophila eye. Genetics *123*, 503-509.

Schneider, C.A., Rasband, W.S., and Eliceiri, K.W. (2012). NIH Image to ImageJ: 25 years of image analysis. Nat Methods *9*, 671-675.

Schottenfeld-Roames, J., and Ghabrial, A.S. (2012). Whacked and Rab35 polarize dynein-motor-complex-dependent seamless tube growth. Nat Cell Biol *14*, 386-393.

Schottenfeld-Roames, J., Rosa, J.B., and Ghabrial, A.S. (2014). Seamless tube shape is constrained by endocytosis-dependent regulation of active Moesin. Curr Biol *24*, 1756-1764.

Schottenfeld, J., Song, Y., and Ghabrial, A.S. (2010). Tube continued: morphogenesis of the Drosophila tracheal system. Curr Opin Cell Biol *22*, 633-639.

Silver, D.L., Geisbrecht, E.R., and Montell, D.J. (2005). Requirement for JAK/STAT signaling throughout border cell migration in Drosophila. Development *132*, 3483-3492.

Sotillos, S., Diaz-Meco, M.T., Moscat, J., and Castelli-Gair Hombria, J. (2008). Polarized subcellular localization of Jak/STAT components is required for efficient signaling. Curr Biol *18*, 624-629.

Sriskanthadevan-Pirahas, S., Turingan, M.J., Chahal, J.S., Thorson, E., Khan, S., Tinwala, A.Q., and Grewal, S.S. (2022). Adipose mitochondrial metabolism controls body growth by modulating systemic cytokine and insulin signaling. Cell Rep *39*, 110802.

Stenmark, H. (2009). Rab GTPases as coordinators of vesicle traffic. Nat Rev Mol Cell Biol *10*, 513-525.

Strutt, H., and Strutt, D. (2021). How do the Fat-Dachsous and core planar polarity pathways act together and independently to coordinate polarized cell behaviours? Open Biol *11*, 200356.

Tamamouna, V., Rahman, M.M., Petersson, M., Charalambous, I., Kux, K., Mainor, H., Bolender, V., Isbilir, B., Edgar, B.A., and Pitsouli, C. (2021). Remodelling of oxygen-transporting tracheoles drives intestinal regeneration and tumorigenesis in Drosophila. Nat Cell Biol *23*, 497-510.

Taylor, J., Abramova, N., Charlton, J., and Adler, P.N. (1998). Van Gogh: a new Drosophila tissue polarity gene. Genetics *150*, 199-210.

Thomas, C., and Strutt, D. (2012). The roles of the cadherins Fat and Dachsous in planar polarity specification in Drosophila. Dev Dyn *241*, 27-39.

Tree, D.R., Shulman, J.M., Rousset, R., Scott, M.P., Gubb, D., and Axelrod, J.D. (2002). Prickle

921 mediates feedback amplification to generate asymmetric planar cell polarity signaling. Cell *109*, 371-
922 381.
923 Tsurumi, A., Xia, F., Li, J., Larson, K., LaFrance, R., and Li, W.X. (2011). STAT is an essential
924 activator of the zygotic genome in the early Drosophila embryo. PLoS Genet *7*, e1002086.
925 Verboogen, D.R.J., Ter Beest, M., Honigmann, A., and van den Bogaart, G. (2018). Secretory vesicles
926 of immune cells contain only a limited number of interleukin 6 molecules. FEBS Lett *592*, 1535-1544.
927 Vinson, C.R., and Adler, P.N. (1987). Directional non-cell autonomy and the transmission of polarity
928 information by the frizzled gene of Drosophila. Nature *329*, 549-551.
929 Vitorino, P., and Meyer, T. (2008). Modular control of endothelial sheet migration. Genes Dev *22*,
930 3268-3281.
931 Vonderheit, A., and Helenius, A. (2005). Rab7 associates with early endosomes to mediate sorting and
932 transport of Semliki forest virus to late endosomes. PLoS Biol *3*, e233.
933 Wang, Y., Yang, Q., Meng, X., Wijaya, C.S., Ren, X., and Xu, S. (2022). Recruitment of tetraspanin
934 TSP-15 to epidermal wounds promotes plasma membrane repair in C. elegans. Dev Cell *57*, 1630-1642
935 e1634.
936 Williams, A.M., Donoughe, S., Munro, E., and Horne-Badovinac, S. (2022). Fat2 polarizes the WAVE
937 complex in trans to align cell protrusions for collective migration. Elife *11*.
938 Wong, L.L., and Adler, P.N. (1993). Tissue polarity genes of Drosophila regulate the subcellular
939 location for prehair initiation in pupal wing cells. J Cell Biol *123*, 209-221.
940 Woodcock, K.J., Kierdorf, K., Pouchelon, C.A., Vivancos, V., Dionne, M.S., and Geissmann, F. (2015).
941 Macrophage-derived upd3 cytokine causes impaired glucose homeostasis and reduced lifespan in
942 Drosophila fed a lipid-rich diet. Immunity *42*, 133-144.
943 Wulff, J., and Black, M.J. (2015). Efficient sparse-to-dense optical flow estimation using a learned
944 basis and layers. Paper presented at: 2015 IEEE Conference on Computer Vision and Pattern
945 Recognition (CVPR).
946 Yang, C.H., Axelrod, J.D., and Simon, M.A. (2002). Regulation of Frizzled by fat-like cadherins during
947 planar polarity signaling in the Drosophila compound eye. Cell *108*, 675-688.
948 Yoshihara, M., Adolfsen, B., Galle, K.T., and Littleton, J.T. (2005). Retrograde signaling by Syt 4
949 induces presynaptic release and synapse-specific growth. Science *310*, 858-863.
950 Zallen, J.A. (2007). Planar polarity and tissue morphogenesis. Cell *129*, 1051-1063.
951 Zeidler, M.P., Bach, E.A., and Perrimon, N. (2000). The roles of the Drosophila JAK/STAT pathway.
952 Oncogene *19*, 2598-2606.
953 Zeidler, M.P., Perrimon, N., and Strutt, D.I. (1999). Polarity determination in the Drosophila eye: a
954 novel role for unpaired and JAK/STAT signaling. Genes Dev *13*, 1342-1353.
955 Zhao, Q., Wirka, R., Nguyen, T., Nagao, M., Cheng, P., Miller, C.L., Kim, J.B., Pjanic, M., and
956 Quertermous, T. (2019). TCF21 and AP-1 interact through epigenetic modifications to regulate
957 coronary artery disease gene expression. Genome Med *11*, 23.
958 Zhao, X., and Karpac, J. (2017). Muscle Directs Diurnal Energy Homeostasis through a Myokine-
959 Dependent Hormone Module in Drosophila. Curr Biol *27*, 1941-1955 e1946.
960 Zheng, H., Yang, X., and Xi, Y. (2016). Fat body remodeling and homeostasis control in Drosophila.
961 Life Sci *167*, 22-31.
962 Zhou, B., Feng, C., Sun, S., Chen, X., Zhuansun, D., Wang, D., Yu, X., Meng, X., Xiao, J., Wu, L.*, et*
963 *al.* (2024). Identification of signaling pathways that specify a subset of migrating enteric neural crest
964 cells at the wavefront in mouse embryos. Dev Cell.

Data availability

The mass spectrometry proteomics data have been deposited to the ProteomeXchange Consortium (https://www.iprox.cn/page/PSV023.html;?url=1708323921277ZyfC) via the iProX partner repository (Ma et al., 2019) with accession number gfnR. The RNA-Seq data generated and analyzed in this study have been deposited in the NCBI database under accession number GSE256177 with token code: clyfasuctboflat. The SMART-Seq data (L3, 0hr APF and 2hr APF) analyzed in this study have been deposited in the NCBI database under accession number GSE184856 [https://www.ncbi.nlm.nih.gov/geo/query/acc.cgi?acc=GSE184856]. The ChIP-Seq data generated and analyzed in this study have been deposited in the NCBI database under accession code 256176 with token: qvupguyijvyndyf.

976 **Figure legends**

977 **Figure 1 Fat body affects disciplined migration of tracheal progenitors.** (A)
978 Schematic cartoon showing the migration of tracheal progenitors (red) and
979 degenerative tracheal branches (dashed grey lines) in pupae. Fat body is shown in
980 beige. Arrows denote anterior-posterior (A-P) axis. (B, C) Frontal section (B) and
981 sagittal view (C) showing the relative position of fat body and tracheal progenitors.
982 (D-J') Migration of tracheal progenitors in control and fat body perturbation flies. (D-
983 D'') Migration of tracheal progenitors (red) upward from transverse connective (blue
984 dashed lines) and along the dorsal trunk (white dotted lines) at 0hr APF (D), 1hr APF
985 (D'), and 3hr APF (D''). (E-E'') Bidirectional movement of tracheal progenitors in fat
986 body-depleted (*lsp2>rpr.hid*) flies. 0hr APF (E), 1hr APF (E'), 3hr APF (E''). Arrows
987 point to anterior movement of tracheal progenitors. (F) Bar graph showing the
988 migration distance of tracheal progenitors. The top chart of column represents the
989 migration distance of anterior-most stem cells, and the lower chart of column
990 represents the migration distance of posterior-most stem cells. Error bars represent
991 SEM, n=6. (G-G') The distribution of progenitors at 2hr APF. (H-H'') The distribution
992 of progenitors in fat body-depleted flies at 2hr APF. (I-J') Computer simulation
993 depicting trajectories of progenitor migration. (I, J) Confocal images of tracheal
994 progenitors. (I', J') Vectors of progenitor migration. (K) Bar graph plots the binary
995 entropy that represents the disorderedness of migration direction of tracheal
996 progenitors. Error bars represent SEM, n=10. (L) The Bernoulli random variable X
997 showing optic flow distribution of the binarized directions in each group. Error bars
998 represent SEM, n=10. N.S. indicates not significant. Scale bar: 100 μm (B, C, G), 200
999 μm (D-E''). Genotypes: (B, C) *UAS-mCD8-GFP/+; lsp2-Gal4,P[B123]-RFP-moe/+*;
1000 (D-D'', G, G') *Gal80^{ts}/+;lsp2-Gal4,P[B123]-RFP-moe/+* ; (E-E'', H, H') *UAS-rpr-*
1001 *hid/+;Gal80^{ts}/+;lsp2-Gal4,P[B123]-RFP-moe/+*.
1002

1003 **Figure 2 Dependence of tracheal progenitors on cytokines from fat body.** (A) Top
1004 functional clusters among the differentially expressed genes of progenitors between

1005 control and fat body-depleted pupae. Gene ratio refers to the proportion of genes in a
1006 dataset that are associated with a particular biological process, function, or pathway.
1007 Count indicates the number of genes from an input gene list that are associated with a
1008 specific GO term. (B) Heatmap depicting expression levels of principal target genes of
1009 signaling pathways in L3 larvae, 0hr APF pupae and 2hr APF pupae. (C) Heatmap
1010 showing the differential expression of target genes of signaling pathways between
1011 control and fat body-depleted pupae. (D-D'') Migration of tracheal progenitors along
1012 the dorsal trunk at 0hr APF (D), 1hr APF (D'), and 3hr APF (D''). The white dashed
1013 line shows transverse connective. (E-E''). Migration of tracheal progenitors in
1014 *upd2RNAi* flies. (F) Bar graph plots the migration distance of tracheal progenitors.
1015 Error bars represent SEM, n=6. (G) Volcano plot showing surface proteomics of
1016 tracheal epithelium (up-regulated genes with ten-fold or higher changes in red; down-
1017 regulated genes with ten-fold or higher changes in blue). (H) Top functional classes
1018 among the surface proteomics of trachea. (I) Schematic diagram depicting the
1019 working principle of the DIPF reporter. (J) The signal of DIPF reporter in tracheal
1020 progenitors. The progenitors are outlined by dashed lines. N.S. indicates not
1021 significant. Scale bar: 200 μm (D-E''), 50 μm (J). Genotypes: (A, C) *lsp2-*
1022 *Gal4,P[B123]-RFP-moe/*+for control*, UAS-rpr-hid/+;Gal80^{ts}/+;lsp2-Gal4,P[B123]-*
1023 *RFP-moe/*+; (B) *P[B123]-RFP-moe/*+. (D-D'') *lsp2-Gal4,P[B123]-RFP-moe/*+; (E-
1024 E'') *lsp2-Gal4,P[B123]-RFP-moe/UAS-upd2RNAi*; (J) *btl-Gal4/UAS-DIPF*.
1025

1026 **Figure 3 JAK/STAT pathway is required for the discipline of tracheal progenitor**
1027 **migration.** (A-D'') Migration of tracheal progenitors along the dorsal trunk at 0hr
1028 APF, 1hr APF and 3hr APF. The white dashed line shows transverse connective. The
1029 progenitors of control (A-A''), *domeRNAi* (B-B''), *hopRNAi* (C-C''), and
1030 *stat92ERNAi* (D-D'') flies. (E) Bar graph showing migration distance of progenitors.
1031 Error bars represent SEM, n=6. (F-G'') JAK inhibition causes bidirectional movement
1032 of progenitors. Migration of tracheal progenitors in the absence (DMSO-fed) (F-F'')
1033 or in the presence of Tofacinib (JAK inhibitor) (G-G''). (H) Bar graph showing the
1034 distance of anterior movement. Error bars represent SEM, n=6. Scale bar: 200 μm (A-

1035 D”, F-G”). Genotypes: (A-A”, F-G”) *btl-Gal4/+;P[B123]-RFP-moe/+*; (B-B”) *btl-*
1036 *Gal4/+;P[B123]-RFP-moe/UAS-domeRNAi*; (C-C”) *btl-Gal4/+;P[B123]-RFP-*
1037 *moe/UAS-hopRNAi*; (D-D”) *btl-Gal4/+;P[B123]-RFP-moe/UAS-stat92ERNAi*.
1038
1039 **Figure 4 Identification of gene targets of Stat92E in *Drosophila* tracheal**
1040 **progenitors.** (A) Bubble plot represents the top functional clusters among gene
1041 targets. The establishment of planar polarity denoted in red solid box is identified with
1042 high enrichment score. (B) Top functional classes among the differentially expressed
1043 genes in larval-pupal transition. (C) ChIP-seq peaks at loci regulated by Stat92E.
1044 Scale bar: 20kb (*ds*, *fz*, *stan*), 5kb (*fat2*, *vg*), 1kb (*fj*). (D-H) Validation of gene targets
1045 of Stat92E ChIP-seq. (D-G) The expression of Ds-GFP in the tracheal progenitors of
1046 control (D), *domeRNAi* (E), *hopRNAi* (F) and *stat92ERNAi* (G). The progenitors are
1047 outlined by dashed lines. (H) The bar graphs plot the relative level of Ds. Error bars
1048 represent SEM, n=6. (I-M) The expression of Fj in tracheal progenitors. The
1049 expression of Fj-GFP in the tracheal progenitors of control (I), *domeRNAi* (J),
1050 *hopRNAi* (K) and *stat92ERNAi* (L). Dashed lines outline tracheal progenitors. (M)
1051 The bar graphs plot the relative level of Fj. Error bars represent SEM, n=6. (N-R) The
1052 level of Ft-GFP in the tracheal progenitors of control (N), *domeRNAi* (O), *hopRNAi*
1053 (P) and *stat92ERNAi* (Q). (R) The bar graphs plot the relative level of Ft. Error bars
1054 represent SEM, n=4. Scale bar: 50 μm (D-G, I-L, N-Q). Genotypes: (D) *btl-Gal4,Ds-*
1055 *GFP/+*; (E) *btl-Gal4,Ds-GFP/+;UAS-domeRNAi/+*; (F) *btl-Gal4,Ds-GFP/+;UAS-*
1056 *hopRNAi/+*; (G) *btl-Gal4,Ds-GFP/+;UAS-stat92ERNAi/+*; (I) *btl-Gal4,Fj-GFP/+*; (J)
1057 *btl-Gal4,Fj-GFP/+;UAS-domeRNAi/+*; (K) *btl-Gal4,Fj-GFP/+;UAS-hopRNAi/+*; (L)
1058 *btl-Gal4,Fj-GFP/+;UAS-stat92ERNAi/+*; (N) *btl-Gal4/+;Ft-GFP/+*; (O) *btl-*
1059 *Gal4/+;Ft-GFP/UAS-domeRNAi*; (P) *btl-Gal4/+;Ft-GFP/UAS-hopRNAi*; (Q) *btl-*
1060 *Gal4/+;Ft-GFP/UAS-stat92ERNAi*.
1061
1062 **Figure 5 Disciplined migration requires planar cell polarity system.** (A-E)
1063 Migration of tracheal progenitors. The migration of progenitors in control (A-A”),
1064 *dsRNAi* (B-B”), *ftRNAi* (C-C”) and *fjRNAi* (D-D”) flies. (E) Bar graph plots the

1065 migration distance of anterior movement. Error bars represent SEM, n=4. (F-I) Level
1066 of Ft in tracheal progenitors of control (F, G) and *stat92ERNAi* (H-J) flies. The
1067 images show progenitors at 1hr APF (H, H') and 2hr APF (I, I'). Ft-GFP (green) (F,
1068 H, I), phalloidin (magenta), Hoechst (blue), and merged images (F', H', I'). (G, J)
1069 Profile plots showing the level of Ft-GFP in control (G) and *stat92ERNAi* (J) flies,
1070 n=5. ANOVA test: $p < 0.0001$. The levels of Ft were measured along the dotted lines
1071 in F' or I'. Anterior (A) and posterior (P). (K) Representative traces plot the migration
1072 distance relative to the origin, n=12. The x-axis represents the number of captured
1073 images. Individual frame is captured every 5 minutes. (K') Rose plot depicting the
1074 direction of cell movement. (L) Representative traces showing the movement of
1075 individual *fj*-KO cells relative to their origin, n=11. The x-axis represents the number
1076 of captured images. Individual frame is captured every 5 minutes. (L') Rose plot
1077 depicting the movement direction of *fj*-KO cells. (M) Scatter plots represent the ratio
1078 (d/D) of straight-line length displacement (d) relative to the length of the migration
1079 track (D) of individual cell. Error bars represent SEM. N.S. indicates not significant.
1080 Scale bar: 200 μm (A-D''), 50 μm (F, F'), 100 μm (H-I'). Genotypes: (A-A'') *btl-*
1081 *Gal4/+;P[B123]-RFP-moe/+*; (B-B'') *btl-Gal4/UAS-dsRNAi;P[B123]-RFP-moe/+*;
1082 (C-C'') *btl-Gal4/+;P[B123]-RFP-moe/UAS-ftRNAi*; (D-D'') *btl-Gal4/UAS-*
1083 *fjRNAi;P[B123]-RFP-moe/+*; (F, F') *btl-Gal4/+;Ft-GFP/+*; (H, H', I, I') *btl-*
1084 *Gal4/+;Ft-GFP/UAS-stat92ERNAi*.
1085
1086 **Figure 6 The production and transport of Upd2 from fat body.** (A, B) The
1087 number of Upd2-mCherry-containing vesicles in fat body of control (DMSO-fed, A)
1088 and BFA-treated L3 larvae (B). Larger view in lower magnification is provided in
1089 Figure 6-figure supplement 1. (C) Bar graph plots the number of Upd2-mCherry-
1090 containing vesicles in fat body. Error bars represent SEM, n=6. (D, E) The confocal
1091 image showing the number of Upd2-containing vesicles in progenitors of DMSO-fed
1092 control (D) and BFA-treated flies (E). (F) Bar graph plots the number of Upd2-
1093 mCherry-containing vesicles in progenitors. Error bars represent SEM, n=4. (G) The
1094 number of Upd2-mCherry containing vesicles (red) in fat body. (H, I) Upd2

1095 accumulation in fat body was increased in the presence of *grasp65RNAi* (H) and
1096 *lbmRNAi* (I). (J) Bar graph plots the number of Upd2-mCherry-containing vesicles.
1097 Error bars represent SEM, n=4. (K-M) The Upd2 vesicles (red) in tracheal progenitors
1098 (DAPI) in control (K), *grasp65RNAi* (L) and *lbmRNAi* (M) flies. Dashed lines outline
1099 tracheal progenitors. (N) Bar graph plots the number of Upd2-mCherry-containing
1100 vesicles in progenitors. Error bars represent SEM, n=4. Scale bar: 20 μm (A, B, G-I),
1101 50 μm (D, E, K-M). Genotypes: (A-G, K) *UAS-upd2-mCherry/+;lsp2-Gal4/+*; (H, L)
1102 *UAS-upd2-mCherry/UAS-grasp65RNAi;lsp2-Gal4/+*; (I, M) *UAS-upd2-*
1103 *mCherry/+;lsp2-Gal4/UAS-lbmRNAi*.
1104
1105 **Figure 7 The dependence of tracheal progenitors on vesicle trafficking.** (A-E)
1106 The expression of Stat92E-GFP in tracheal progenitors of control (A), *grasp65RNAi*
1107 (B), *lbmRNAi* (C), *rab5RNAi* (D) and *rab7RNAi* (E) flies. The progenitors are outlined
1108 by dashed lines. (F) Bar graph plots the relative expression of Stat92E-GFP. Error bars
1109 represent SEM, n=7. (G, H) The expression of Stat92E-GFP in tracheal progenitors in
1110 DMSO-fed (G) and BFA-treated (H) flies. (I) Bar graph plots the relative expression
1111 of Stat92E-GFP. Error bars represent SEM, n=5. (J) The signal of DIPF reporter in
1112 tracheal progenitors. (K) The effects of Tofacinib (JAK inhibitor) on DIPF reporter in
1113 progenitors. (L) The effects of Brefeldin A on DIPF reporter in progenitors. Dashed
1114 lines outline tracheal progenitors. (M) Bar graphs showing the signal of DIPF
1115 reporter. Error bars represent SEM, n=4. (N-O'') Migration of tracheal progenitors in
1116 DMSO-fed flies (N-N'') and BFA-treated flies (O-O''). (P) Bar graph plots migration
1117 distance of anterior movement. Error bars represent SEM, n≥3. (Q-U'') Migration of
1118 tracheal progenitors at 0hr APF (Q), 1hr APF (Q'), 3hr APF (Q''). The confocal
1119 images showing the tracheal progenitors in control (Q-Q''), *grasp65RNAi* (R-R''),
1120 *lbmRNAi* (S-S''), *rab5RNAi* (T-T'') and *rab7RNAi* (U-U'') flies. (V) Bar graph plots
1121 the migration distance of anterior movement. Error bars represent SEM, n=4. Scale
1122 bar: 50 μm (A-E, G, H, J-L), 200 μm (N-O'', Q-U''). Genotypes: (A, G, H) *lsp2-*
1123 *Gal4,Stat92E-GFP/+*; (B) *UAS-grasp65RNAi/+;lsp2-Gal4,Stat92E-GFP/+*; (C) *lsp2-*
1124 *Gal4,Stat92E-GFP/UAS-lbmRNAi*; (D) *UAS-rab5RNAi/+;lsp2-Gal4,Stat92E-GFP/+*;

1125 (E) *UAS-rab7RNAi/+;lsp2-Gal4,Stat92E-GFP/+*; (J-L) *btl-Gal4/UAS-DIPF*; (N-Q'')
1126 *lsp2-Gal4,P[B123]-RFP-moe/+*; (R-R'') *lsp2-Gal4,P[B123]-RFP-moe/UAS-*
1127 *grasp65RNAi*; (S-S'') *lsp2-Gal4,P[B123]-RFP-moe/+;UAS-lbmRNAi/+*; (T-T'')
1128 *UAS-rab5RNAi/+;lsp2-Gal4,P[B123]-RFP-moe/+*; (U-U'') *UAS-rab7RNAi/+;lsp2-*
1129 *Gal4,P[B123]-RFP-moe/+*.
1130
1131 **Figure 8 The roles of endocytic trafficking system in the transport of Upd2.** (A-
1132 D''') The confocal images showing the colocalization between Upd2 (red) (A, B, C,
1133 D) and Rab5 (GFP) (A'), Rab7 (GFP) (B'), Grasp65 (GFP) (C') or Lbm (GFP). (A'',
1134 B'', C'', D'') Merged images. (D''') 3D high-magnification view of the boxed inset in
1135 D''. (D'''') The Pearson's correlation coefficient depicting colocalization between
1136 Lbm and Upd2 in fat body cells. (E-J) The PLA (Proximity Ligation Assay) assay
1137 showing the interaction between Upd2 and Rab5 (E, F), Rab7 (G, H) or Lbm (I, J).
1138 (K-M) Co-immunoprecipitation assay showing physical interaction between Upd2
1139 and Rab5 (K), Rab7 (L) or Lbm (M) in larval fat body. (N-T) The expression of Lbm-
1140 pHluorin in larval fat body and progenitors of control (N, O), *rab5RNAi* (P, Q) and
1141 *rab7RNAi* (R, S) flies. Dashed lines outline tracheal progenitors. Arrowheads point to
1142 Lbm-pHluorin puncta. DAPI signal indicates nuclei. (T) Schematic diagram depicting
1143 Upd2-operated disciplined migration of tracheal progenitors. Scale bar: 5 μm (A-D'',
1144 E-J), 10 μm (N, P, R), 20 μm (O, Q, S). Genotypes: (A-A'', E, F) *UAS-upd2-*
1145 *mCherry/+;lsp2-Gal4/UAS-GFP-rab5*; (B-B'', G, H) *UAS-upd2-mCherry/+;lsp2-*
1146 *Gal4/UAS-GFP-rab7*; (C-C'') *UAS-upd2-mCherry/UAS-grasp65-GFP;lsp2-Gal4/+*;
1147 (D-D'''', I-L) *UAS-upd2-mCherry/UAS-lbm-GFP;lsp2-Gal4/+*; (N, O) *UAS-lbm-*
1148 *pHluorin/+;lsp2-Gal4/+*; (P, Q) *UAS-lbm-pHluorin/UAS-rab5RNAi;lsp2-Gal4/+*; (R,
1149 S) *UAS-lbm-pHluorin/UAS-rab7RNAi;lsp2-Gal4/+*.
1150
1151 **Figure 1-figure supplement 1 Genetic perturbation of fat body by expression of**
1152 **pro-apoptotic genes, *rpr* and *hid*.** Confocal images of larval fat body in control (A)
1153 and *lsp2>rpr.hid* (B) animals. Microscopic pictures of control (C) and *lsp2>rpr.hid*
1154 larvae (D). (E) Scatter plot showing migration velocity of tracheal progenitors in

1155 control and *lsp2>rpr.hid* animals. Error bars represent SEM, n=6. (F, G) The
1156 incorporation of EdU in the tracheal progenitors of control (F) and *lsp2>rpr.hid*
1157 animals (G). (H) Bar graph depicting the number of EdU incorporation. Error bars
1158 represent SEM, n=11. Scale bar: 100 μm (A, B), 20 μm (C, D), 50 μm (F, G).
1159 Genotypes: (A, C, F) *lsp2-Gal4,P[B123]-RFP-moe/+*; (B, D) *UAS-rpr.hid/+;lsp2-*
1160 *Gal4,P[B123]-RFP-moe/+*; (G) *UAS-rpr.hid/+;Gal80^{ts}/+;lsp2-Gal4,P[B123]-RFP-*
1161 *moe/+*.
1162
1163 **Figure 2-figure supplement 1 Identification of genes that contribute to**
1164 **progenitors migration.** (A) Differentially expressed genes in tracheal progenitors of
1165 *lsp2>rpr.hid* pupa compared with control. (B) Volcano plot of RNA-seq showing
1166 differentially regulated genes with 2-fold or higher changes (up-regulated genes in
1167 red; down-regulated genes in blue) in *lsp2>rpr.hid* compared with control. (C-I") The
1168 migration of progenitors at 0hr APF, 1hr APF, or 3hr APF in control (C-C") and
1169 *upd1RNAi* (D-D"), *upd3RNAi* (E-E"), *pvf1RNAi* (F-F"), *pvf2RNAi* (G-G"), *pvf3RNAi*
1170 (H-H"), and *hhRNAi* (I-I"). (J) Bar graph represents the migration distance of anterior
1171 movement. Error bars represent SEM, n=4. (K) The migration of progenitors in
1172 control (K-K") and *btl>upd2RNAi* (L-L"). (M) Bar graph plots the migration distance
1173 of anterior movement. Error bars represent SEM, n=4. N.S. indicates not significant.
1174 Scale bar: 200 μm (C-I", K-L"). Genotypes: (C-C") *lsp2-Gal4,P[B123]-RFP-moe/+*;
1175 (D-D") *lsp2-Gal4,P[B123]-RFP-moe/UAS-upd1RNAi*; (E-E") *lsp2-Gal4,P[B123]-*
1176 *RFP-moe/UAS-upd3RNAi*; (F-F") *lsp2-Gal4,P[B123]-RFP-moe/UAS-pvf1RNAi*; (G-
1177 G") *lsp2-Gal4,P[B123]-RFP-moe/UAS-pvf2RNAi*; (H-H") *lsp2-Gal4,P[B123]-RFP-*
1178 *moe/UAS-pvf3RNAi*; (I-I") *lsp2-Gal4,P[B123]-RFP-moe/UAS-hhRNAi*; (K-K") *btl-*
1179 *Gal4/+;P[B123]-RFP-moe/+*; (L-L") *btl-Gal4/+;P[B123]-RFP-moe/UAS-upd2RNAi*.
1180
1181 **Figure 2-figure supplement 2 Surface proteomics of *Drosophila* trachea.** (A-C)
1182 Representative confocal images showing the trachea of *btl>CD2-HRP* flies after
1183 oxidation reaction in the presence of both BXXP and H_2O_2 (A), BXXP only (B), or
1184 H_2O_2 only (C). (D) The western blot showing the biotinylated proteins labeled by an

1185 HRP-catalyzed reaction with both BXXP and H_2O_2. (E) The confocal image showing
1186 the trachea of *dome>GFP* flies. The expression domain of *dome* is visualized by
1187 *dome*-Gal4-controlled GFP expression. The progenitors labeled by a progenitor-
1188 specific enhancer, P[B123]-RFP-moe are outlined by dashed lines. The overlapping
1189 expression of GFP and P[B123]-RFP-moe. (F, G) The expression of DIPF in fat body
1190 (F) and salivary gland (G). Scale bar: 50 μm (E-H). Genotypes: (A-C) *btl-Gal4/UAS-*
1191 *CD2-HRP*; (E) *dome-Gal4/+;UAS-GFP/P[B123]-RFP-moe*; (F,G) *tub-Gal4/UAS-*
1192 *DIPF*.
1193
1194 **Figure 3-figure supplement 1 The roles of JAK/STAT pathway in tracheal**
1195 **development.** (A-E) Migration of tracheal progenitors along the dorsal trunk at 0hr
1196 APF, 1hr APF and 3hr APF. The white dashed line shows transverse connective. The
1197 progenitors of control (A-A''), *dome* mutants (B-B''), *hop* mutants (C-C''). (D) Bar
1198 graphs represent migration distance of anterior movement. Error bars represent SEM,
1199 n≥3. N.S. indicates not significant. (E-I) The pupal trachea in control (E), *upd2 RNAi*
1200 (F), $dome^{G0264}$ (G), hop^{tum} (H), and $stat92E^{F}$ (I). Scale bar: 200 μm (A-E), 20mm (K-
1201 L''). Genotypes: (A, E) *lsp2-Gal4,P[B123]-RFP-moe/+*(control); (B) $dome^{G0264}$*; lsp2-*
1202 *Gal4,P[B123]-RFP-moe/+*; (C) hop^{tum}*; lsp2-Gal4,P[B123]-RFP-moe/+*; (F) *lsp2-*
1203 *Gal4,P[B123]-RFP-moe/upd2RNAi.* (G) $dome^{G0264}$. (H) hop^{tum}. (I) $stat92E^{F}$.
1204
1205 **Figure 3-figure supplement 2 The dependence of tracheal progenitors on**
1206 **JAK/STAT pathway.** (A) Statistics of the number of progenitor cells. Error bars
1207 represent SEM, n≥9. N.S. indicates not significant. (B-E) The expression of Stat92E-
1208 GFP in tracheal progenitors of control (B), *domeRNAi* (C), *hopRNAi* (D) and
1209 *stat92ERNAi* (E) flies. The progenitors are outlined by dashed lines. (F, G) The
1210 expression of Stat92E-GFP in tracheal progenitors of control (F) or upd2RNAi flies
1211 (G). (H, I) The expression of Stat92E-GFP in tracheal progenitors of DMSO-fed
1212 (control, H) or Tofacitinib-treated (I) flies. Dashed lines outline tracheal progenitors.
1213 (J) Bar graph plots relative intensity of Stat92E-GFP reporter. Error bars represent
1214 SEM, n=6. N.S. indicates not significant. Scale bar: 50 μm (B-I). Genotypes: (A) *btl-*

1215 *Gal4/+;P[B123]-RFP-moe/+*(control); *btl-Gal4/+;P[B123]-RFP-moe/UAS-*
1216 *domeRNAi*; *btl-Gal4/+;P[B123]-RFP-moe/UAS-hopRNAi*; *btl-Gal4/+;P[B123]-RFP-*
1217 *moe/UAS-stat92ERNAi*; (B) *btl-Gal4,Stat92E-GFP/+*; (C) *btl-Gal4,Stat92E-*
1218 *GFP/+;UAS-domeRNAi/+*; (D) *btl-Gal4,Stat92E-GFP/+;UAS-hopRNAi/+*; (E) *btl-*
1219 *Gal4,Stat92E-GFP/+;UAS-Stat92ERNAi/+*; (F, H, I) *Stat92E-GFP/+; lsp2-Gal4/+*;
1220 (G) *Stat92E-GFP/+;lsp2-Gal4/UAS-upd2RNAi*.
1221
1222 **Figure 4-figure supplement 1 Annotation and analysis of genomic occupancy of**
1223 **Stat92E.** (A-C) Pie chart (A, B) and histogram (C) depicting the distribution of ChIP-
1224 seq peaks relative to the nearby annotated genes. (D) Peaks of Stat92E association in
1225 the promotor regions of *yurt* and *crb*. Scale bar: 2kb for *yurt*, 5kb for *crb*. (E) Relative
1226 enrichment of JAK/STAT target genes analyzed by ChIP-qPCR. (F-I) The expression
1227 of Fat2-GFP in the tracheal progenitors of control (F), *domeRNAi* (G), *hopRNAi* (H)
1228 and *stat92ERNAi* (I). The progenitors are outlined by dashed lines. (J) The bar graphs
1229 plot the relative level of Fat2. Error bars represent SEM, n=6. (K-N) The expression
1230 of Yurt in tracheal progenitors. The expression of Yurt-GFP in the tracheal progenitors
1231 of control (K), *domeRNAi* (L), *hopRNAi* (M) and *stat92ERNAi* (N). The progenitors
1232 are outlined by dashed lines. (O) The bar graphs plot the relative level of Yurt. Error
1233 bars represent SEM, n=6. (P-S) The expression of Crb-GFP in the tracheal progenitors
1234 of control (P), *domeRNAi* (Q), *hopRNAi* (R) and *stat92ERNAi* (S). The progenitors are
1235 outlined by dashed lines. (T) The bar graphs plot the relative level of Crb. Error bars
1236 represent SEM, n=6. (U) The expression of JAK/STAT targets in the trachea of
1237 *stat92ERNAi* flies. Quantitative RT-PCR was performed in triplets to analyze the
1238 mRNA level. The expression levels in *stat92ERNAi* larvae were presented relative to
1239 *Gal4* control. Scale bar: 50 μm (F-I, K-N, P-S). Genotypes: (F) *btl-Gal4,Fat2-GFP/+*;
1240 (G) *btl-Gal4,Fat2-GFP/+;UAS-domeRNAi/+*; (H) *btl-Gal4,Fat2-GFP/+;UAS-*
1241 *hopRNAi/+*; (I) *btl-Gal4,Fat2-GFP/+;UAS-stat92ERNAi/+*; (J) *btl-Gal4/+;Yurt-*
1242 *GFP/+*; (K) *btl-Gal4/+;Yurt-GFP/UAS-domeRNAi*; (L) *btl-Gal4/+;Yurt-GFP/UAS-*
1243 *hopRNAi*; (M) *btl-Gal4/+;Yurt-GFP/UAS-stat92ERNAi*; (P) *btl-Gal4/+;Crb-GFP/+*;
1244 (Q) *btl-Gal4/+;Crb-GFP/UAS-domeRNAi*; (R) *btl-Gal4/+;Crb-GFP/UAS-hopRNAi*;

1245 (S) *btl-Gal4/+;Crb-GFP/UAS-stat92ERNAi*.

1246

1247 **Figure 4-figure supplement 2 Ds alters the level of Ft.** (A-C) The level of Ft-GFP
1248 in control (A), UAS-ds (B), and dsRNAi (C) flies. (D) Bar graph represents the signal
1249 of Ft-GFP. Error bars represent SEM, n=4. Scale bar: 50 μm (A-C). Genotypes: (A)
1250 *btl-Gal4/+;Ft-GFP/+*; (B) *btl-Gal4/+;Ft-GFP/UAS-ds*; (C) *btl-Gal4/+;Ft-GFP/UAS-*
1251 *dsRNAi*.

1252

1253 **Figure 5-figure supplement 1 Apico-basal polarity proteins contribute to the**
1254 **migration polarity of progenitors.** (A-H'') The migration of progenitors at 0hr APF
1255 (A), 1hr APF (A'), 3hr APF (A'') in control (A-A''), *UAS-ds* (B-B''), *UAS-ft* (C-C''),
1256 *fat2RNAi* (E-E''), *crbRNAi* (F-F''), *yurtRNAi* (G-G'') and *scbRNAi* (H-H''). (D,I,J)
1257 Bar graph plots the migration distance of anterior movement. Error bars represent
1258 SEM, n≥3. N.S. indicates not significant. Scale bar: 200 μm (A-C'', E-H'').
1259 Genotypes: (A-A'') *btl-Gal4/+;P[B123]-RFP-moe/+*; (B-B'') *btl-*
1260 *Gal4/+;P[B123]/UAS-ds*; (C-C'') *btl-Gal4/UAS-ft;P[B123]/+*; (E-E'') *btl-*
1261 *Gal4/+;P[B123]-RFP-moe/UAS-fat2RNAi*; (F-F'') *btl-Gal4/+;P[B123]-RFP-*
1262 *moe/UAS-crbRNAi*; (G-G'') *btl-Gal4/+;P[B123]-RFP-moe/UAS-yurtRNAi*; (H-H'')
1263 *btl-Gal4/+;P[B123]-RFP-moe/UAS-scbRNAi*. (J) *btl-Gal4/+;P[B123]-RFP-*
1264 *moe/+*(control); *btl-Gal4/+;P[B123]-RFP-moe/UAS-enaRNAi*; *btl-Gal4/ UAS-*
1265 *fakRNAi;P[B123]-RFP-moe/+*; *btl-Gal4/+;P[B123]-RFP-moe/UAS-E-cadRNAi*; *btl-*
1266 *Gal4/+;P[B123]-RFP-moe/UAS-robo2RNAi*.

1267

1268 **Figure 5-figure supplement 2 Protrusions extending from the leading edge of**
1269 **progenitors.** (A, B) The confocal image showing the filopodia at the leading edge of
1270 migrating tracheal progenitors in control (A) and *upd2RNAi* flies (B). Arrows denote
1271 anterior-posterior (A-P) axis. Dashed lines indicate dorsal trunk. (C) Bar graph
1272 depicting the number of filopodia extending from leading edge. Error bars represent
1273 SEM, n=8. (D, E) Expression of *bnl*-lacZ in the trachea of control (D) and
1274 *stat92ERNAi* (E) flies. Scale bar: 100 μm (A, B), 500 μm (D, E). Genotypes: (A) *lsp2-*

1275 *Gal4,P[B123]-RFP-moe/+*; (B) *lsp2-Gal4,P[B123]-RFP-moe/UAS-upd2RNAi*.

1276

1277 **Figure 5-figure supplement 3 The dependence of migration directionality on**
1278 **Ft/Ds system.** (A) Representative traces plot the migration distance relative to the
1279 origin, n≥10. (B) Rose plot depicting the direction of cell movement. (C)
1280 Representative traces showing the movement of individual *dsRNAi* cells relative to
1281 their origin. (D) Rose plot depicting the movement direction of *dsRNAi* cells. (E)
1282 Representative traces showing the movement of individual *ftRNAi* cells relative to
1283 their origin. (F) Rose plot depicting the movement direction of *ftRNAi* cells. (G)
1284 Scatter plots represent the ratio (*d*/*D*) of straight-line length displacement (*d*) relative
1285 to the length of the migration track (*D*) of individual cell.

1286

1287 **Figure 6-figure supplement 1 Microscopic image of a preparation of fly fat body.**
1288 Scale bar: 50 um.

1289

1290 **Figure 7-figure supplement 1 The roles of Rabs in transport of Upd2**. (A-C'')
1291 Migration of tracheal progenitors. The migration of progenitors at 0hr APF, 1hr APF,
1292 3hr APF in control (A-A''), *rab2RNAi* (B-B''), *rab3RNAi* (C-C''). (D) Bar graph plots
1293 the migration distance of anterior movement. Error bars represent SEM, n≥3. (E-E'')
1294 The confocal images showing the colocalization between Upd2 (red) (E) and Rab3
1295 (GFP) (E'). (E'') Merged images. Scale bar: 200 μm (A-C''), 5 μm (E-E'').
1296 Genotypes: (A-A'') *lsp2-Gal4,P[B123]-RFP-moe/+*; (B-B'') *lsp2-Gal4,P[B123]-*
1297 *RFP-moe/UAS-rab2RNAi*; (C-C'') *lsp2-Gal4,P[B123]-RFP-moe/UAS-rab3RNAi*; (E-
1298 E'') *UAS-upd2-mCherry/UAS-rab3-YFP;lsp2-Gal4/+*.

1299

1300 **Figure 8-figure supplement 1 Vesicular transport of Upd2.** (A-C'') Co-
1301 localization and interaction between Lbm and Upd2. Co-transfection of act-Gal4,
1302 UAS-lbm-GFP (A) and UAS-upd2-mCherry (A') in S2 cells. (A'') Merged image. (B-
1303 C'') Confocal images showing that Lbm co-localizes with Upd2 in vesicles along the
1304 protrusions of S2 cell. (D) Electron microscopic image of Lbm-HRP vesicles (dark) in

1305 fat body. (E) A predicted interaction between Lbm (blue) and Upd2 (green). (F) Co-
1306 immunoprecipitation assay showing the interaction between Lbm and Upd2 in S2
1307 cells. (G, H) The expression of Lbm-pHluorin in control fat body (G) and BFA-treated
1308 flies (H). (I, J) The expression of Lbm-pHluorin in control tracheal progenitors (I) and
1309 BFA-treated flies (J). The tracheal progenitors were outlined by dashed lines. Scale
1310 bar: 10 μm (A-A"), 20 μm (G, H). Genotypes: (G-J) *UAS-lbm-pHluorin/+;lsp2-*
1311 *Gal4/+*.
1312
1313 **Video 1 3D-view of confocal image stack of tracheal progenitors and fat body.**
1314 Scale bar: 100 μm. Genotype: *UAS-mCD8-GFP/+;lsp2-Gal4,P[B123]-RFP-moe/+*.
1315
1316 **Video 2 The movement of tracheal progenitors in control and *rpr.hid* flies.** Scale
1317 bar: 100 μm. Genotypes: *Gal80^{ts}/+;lsp2-Gal4,P[B123]-RFP-moe/+* (control) and
1318 *UAS-rpr-hid/+;Gal80^{ts}/+;lsp2-Gal4,P[B123]-RFP-moe/+*.
1319
1320 **Video 3 The movement of tracheal progenitors in control and *upd2RNAi* flies.**
1321 Scale bar: 100 μm. Genotypes: *lsp2-Gal4,P[B123]-RFP-moe/+* (control) and *lsp2-*
1322 *Gal4,P[B123]-RFP-moe/UAS-upd2RNAi*.
1323
1324 **Video 4 The movement of tracheal progenitors in control and JAK/STAT**
1325 **pathway-perturbed flies.** Scale bar: 100 μm. Genotypes: *btl-Gal4/+;P[B123]-RFP-*
1326 *moe/+* (control), *btl-Gal4/+;P[B123]-RFP-moe/UAS-domeRNAi*, *btl-*
1327 *Gal4/+;P[B123]-RFP-moe/UAS-hopRNAi* and *btl-Gal4/+;P[B123]-RFP-moe/UAS-*
1328 *stat92ERNAi*.
1329
1330 **Video 5 The movement of tracheal progenitors in control and PCP component**
1331 **aberrant flies.** Scale bar: 100 μm. Genotypes: *btl-Gal4/+;P[B123]-RFP-*
1332 *moe/+*(control), *btl-Gal4/UAS-dsRNAi;P[B123]-RFP-moe/+* and *btl-*
1333 *Gal4/+;P[B123]-RFP-moe/UAS-ftRNAi*.
1334

1335 **Video 6 The movement of tracheal progenitors in control and *lbmRNAi* flies.**

1336 Scale bar: 100 μm. Genotypes: *lsp2-Gal4,P[B123]-RFP-moe/+* (control) and *lsp2-*

1337 *Gal4,P[B123]-RFP-moe/+;UAS-lbmRNAi/+*.

1338

1339

Figure 1

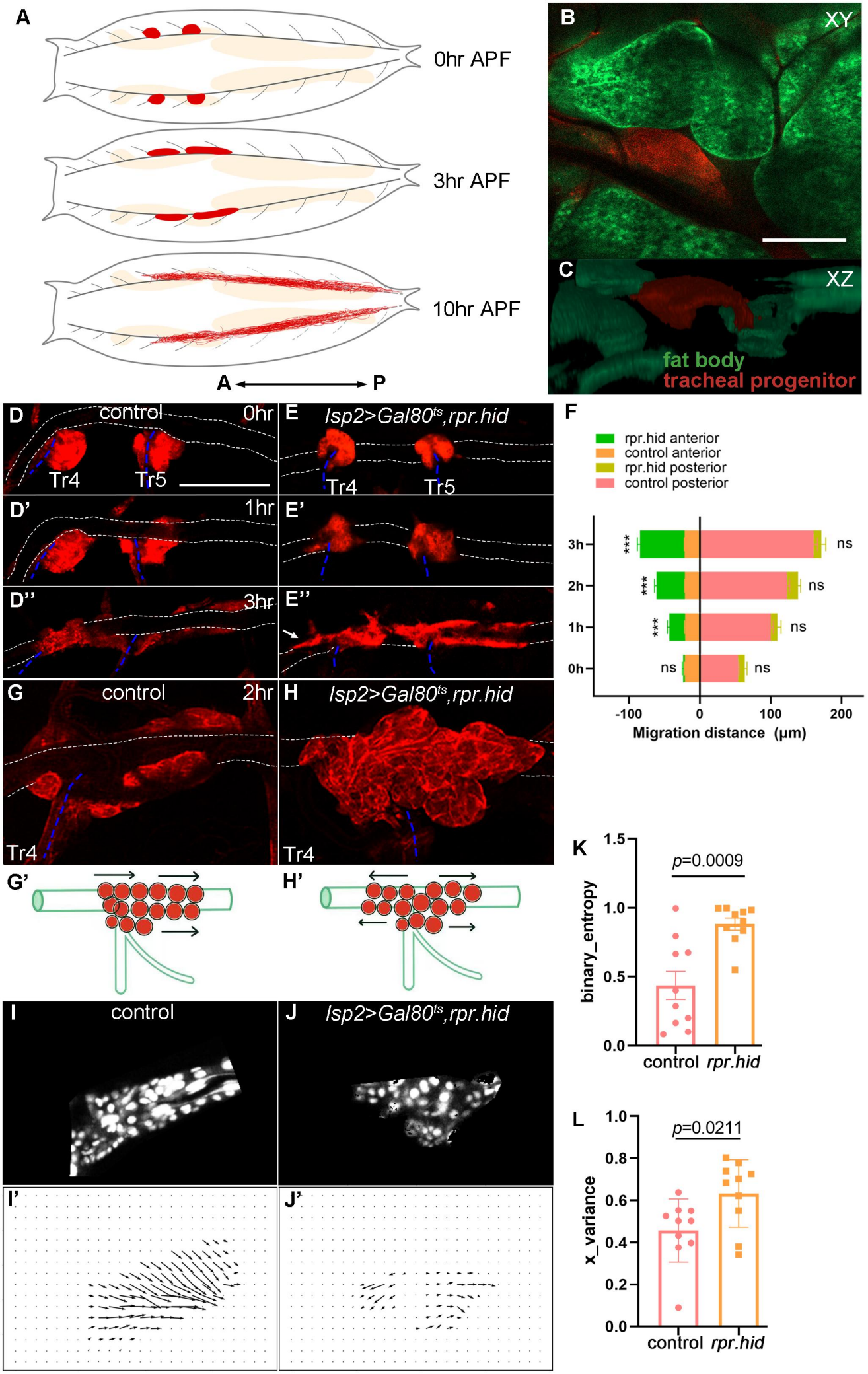
A
0hr APF
3hr APF
10hr APF
A
P
B
XY
C
XZ
fat body
tracheal progenitor
D
control
0hr
Tr4
Tr5
E
lsp2>Gal80ts,rpr.hid
Tr4
Tr5
D'
1hr
E'
D''
3hr
E''
G
control
2hr
Tr4
H
lsp2>Gal80ts,rpr.hid
Tr4
G'
H'
I
control
J
lsp2>Gal80ts,rpr.hid
I'
J'
F
rpr.hid anterior
control anterior
rpr.hid posterior
control posterior
3h
2h
1h
0h
***
ns
-100
0
100
200
Migration distance (μm)
K
p=0.0009
binary_entropy
1.5
1.0
0.5
0.0
control
rpr.hid
L
p=0.0211
x_variance
1.0
0.8
0.6
0.4
0.2
0.0
control
rpr.hid

Figure 2

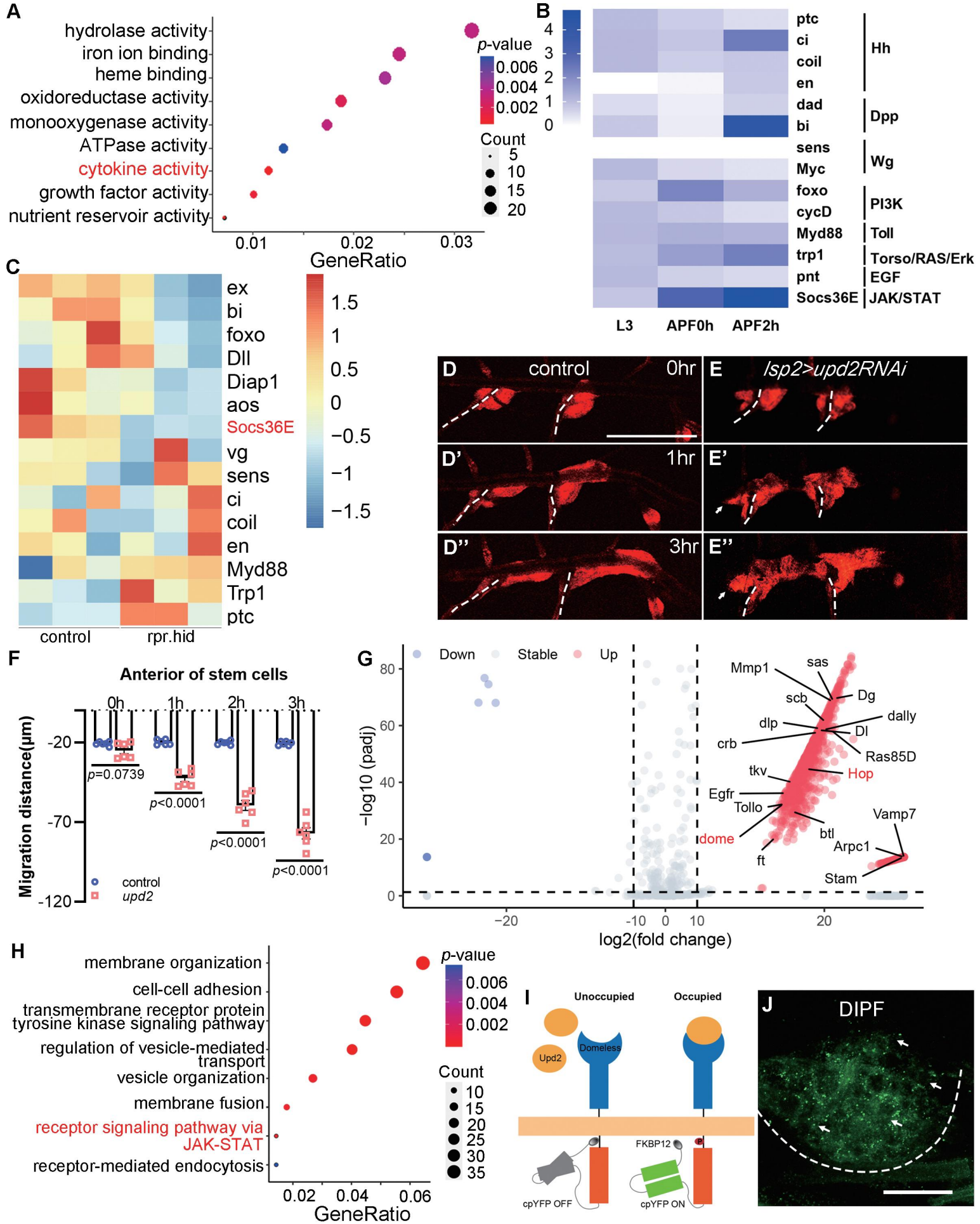
A
hydrolase activity
iron ion binding
heme binding
oxidoreductase activity
monooxygenase activity
ATPase activity
cytokine activity
growth factor activity
nutrient reservoir activity
0.01
0.02
0.03
GeneRatio
p-value
0.006
0.004
0.002
Count
5
10
15
20
B
4
3
2
1
0
ptc
ci
coil
en
dad
bi
sens
Myc
foxo
cycD
Myd88
trp1
pnt
Socs36E
Hh
Dpp
Wg
PI3K
Toll
Torso/RAS/Erk
EGF
JAK/STAT
L3
APF0h
APF2h
C
ex
bi
foxo
Dll
Diap1
aos
Socs36E
vg
sens
ci
coil
en
Myd88
Trp1
ptc
control
rpr.hid
1.5
1
0.5
0
−0.5
−1
−1.5
D
control
0hr
D'
1hr
D''
3hr
E
/sp2>upd2RNAi
E'
E''
F
Anterior of stem cells
0h
1h
2h
3h
Migration distance(μm)
-20
-70
-120
p=0.0739
p<0.0001
p<0.0001
p<0.0001
control
upd2
G
Down
Stable
Up
80
60
40
20
0
−log10 (padj)
−20
-10
0
10
20
log2(fold change)
Mmp1
sas
scb
Dg
dally
dlp
Dl
crb
Ras85D
tkv
Hop
Egfr
Tollo
Vamp7
dome
btl
Arpc1
ft
Stam
H
membrane organization
cell-cell adhesion
transmembrane receptor protein tyrosine kinase signaling pathway
regulation of vesicle-mediated transport
vesicle organization
membrane fusion
receptor signaling pathway via JAK-STAT
receptor-mediated endocytosis
0.02
0.04
0.06
GeneRatio
p-value
0.006
0.004
0.002
Count
10
15
20
25
30
35
I
Unoccupied
Occupied
Upd2
Domeless
FKBP12
P
cpYFP OFF
cpYFP ON
J
DIPF

Figure 3

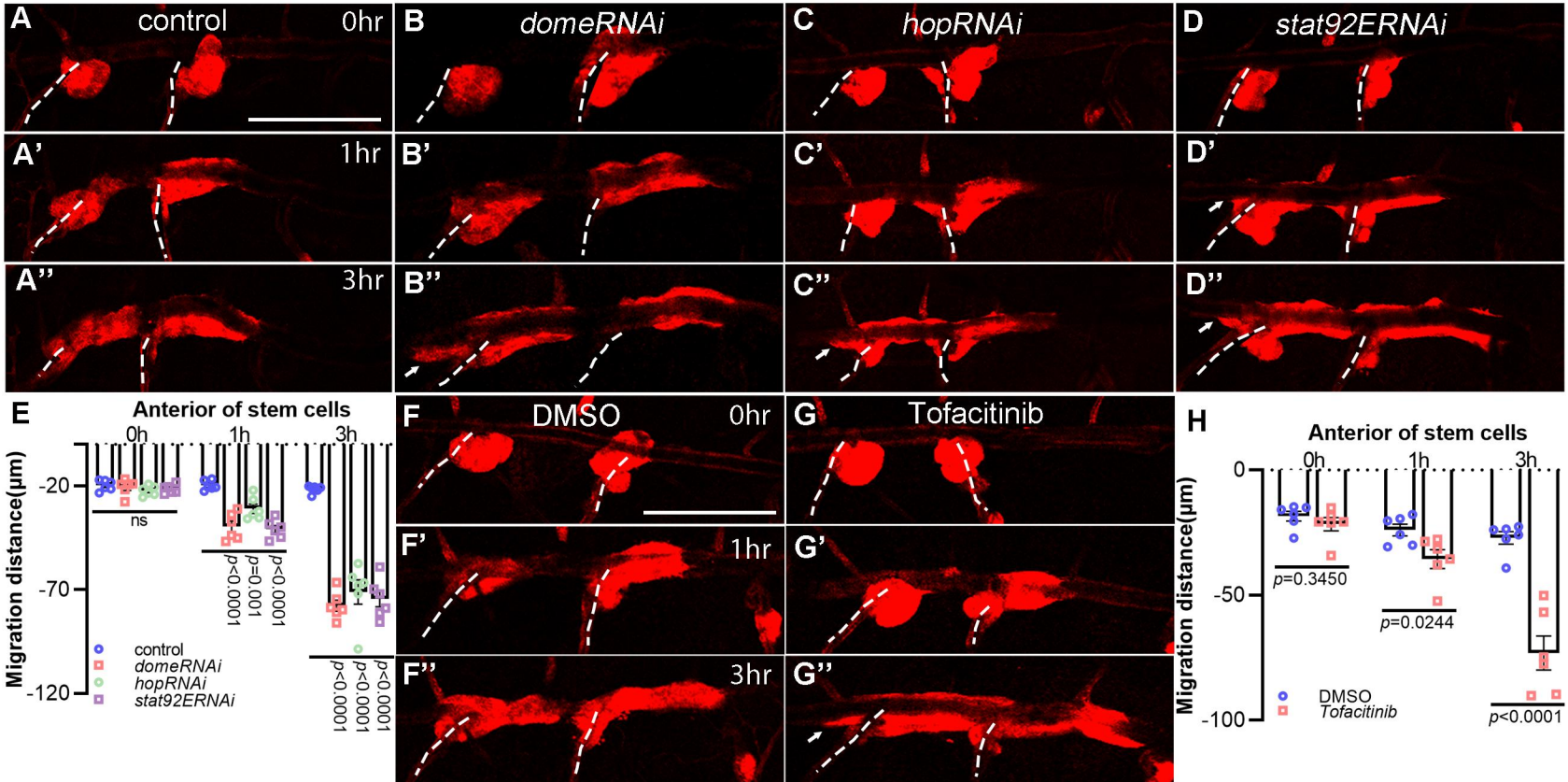
A
control
0hr
B
domeRNAi
C
hopRNAi
D
stat92ERNAi
A'
1hr
B'
C'
D'
A''
3hr
B''
C''
D''
E
Anterior of stem cells
0h
1h
3h
Migration distance(μm)
-20
-70
-120
ns
p<0.0001
p=0.001
p<0.0001
p<0.0001
p<0.0001
p<0.0001
control
domeRNAi
hopRNAi
stat92ERNAi
F
DMSO
0hr
G
Tofacitinib
F'
1hr
G'
F''
3hr
G''
H
Anterior of stem cells
0h
1h
3h
Migration distance(μm)
0
-50
-100
p=0.3450
p=0.0244
p<0.0001
DMSO
Tofacitinib

Figure 4

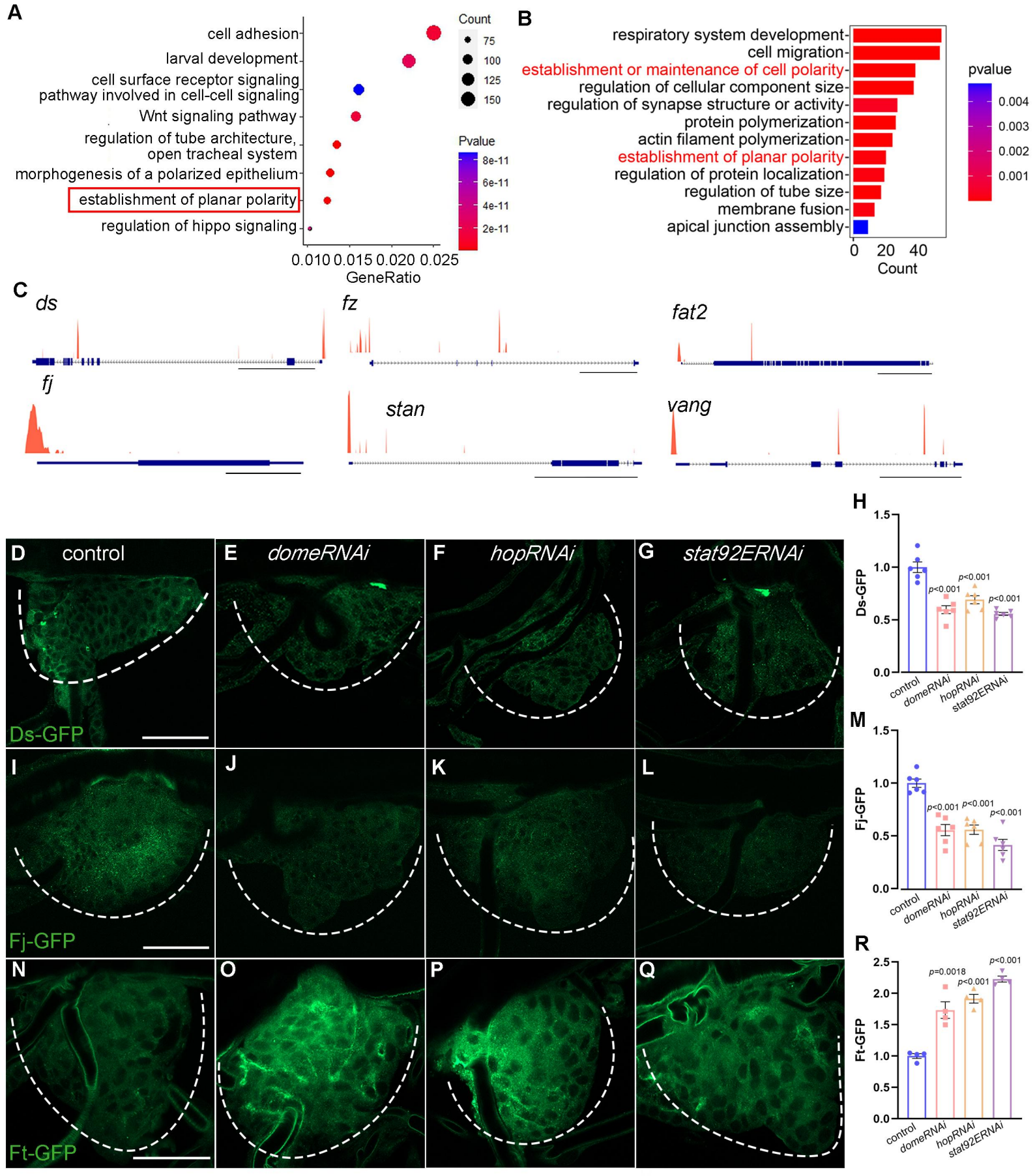
A
cell adhesion
larval development
cell surface receptor signaling pathway involved in cell-cell signaling
Wnt signaling pathway
regulation of tube architecture, open tracheal system
morphogenesis of a polarized epithelium
establishment of planar polarity
regulation of hippo signaling
0.010 0.015 0.020 0.025
GeneRatio
Count
75
100
125
150
Pvalue
8e-11
6e-11
4e-11
2e-11
B
respiratory system development
cell migration
establishment or maintenance of cell polarity
regulation of cellular component size
regulation of synapse structure or activity
protein polymerization
actin filament polymerization
establishment of planar polarity
regulation of protein localization
regulation of tube size
membrane fusion
apical junction assembly
0 20 40
Count
pvalue
0.004
0.003
0.002
0.001
C
ds
fz
fat2
fj
stan
vang
D control
E domeRNAi
F hopRNAi
G stat92ERNAi
Ds-GFP
I
J
K
L
Fj-GFP
N
O
P
Q
Ft-GFP
H
Ds-GFP
p<0.001
p<0.001
p<0.001
control
domeRNAi
hopRNAi
stat92ERNAi
M
Fj-GFP
p<0.001
p<0.001
p<0.001
R
Ft-GFP
p=0.0018
p<0.001
p<0.001

Figure 5

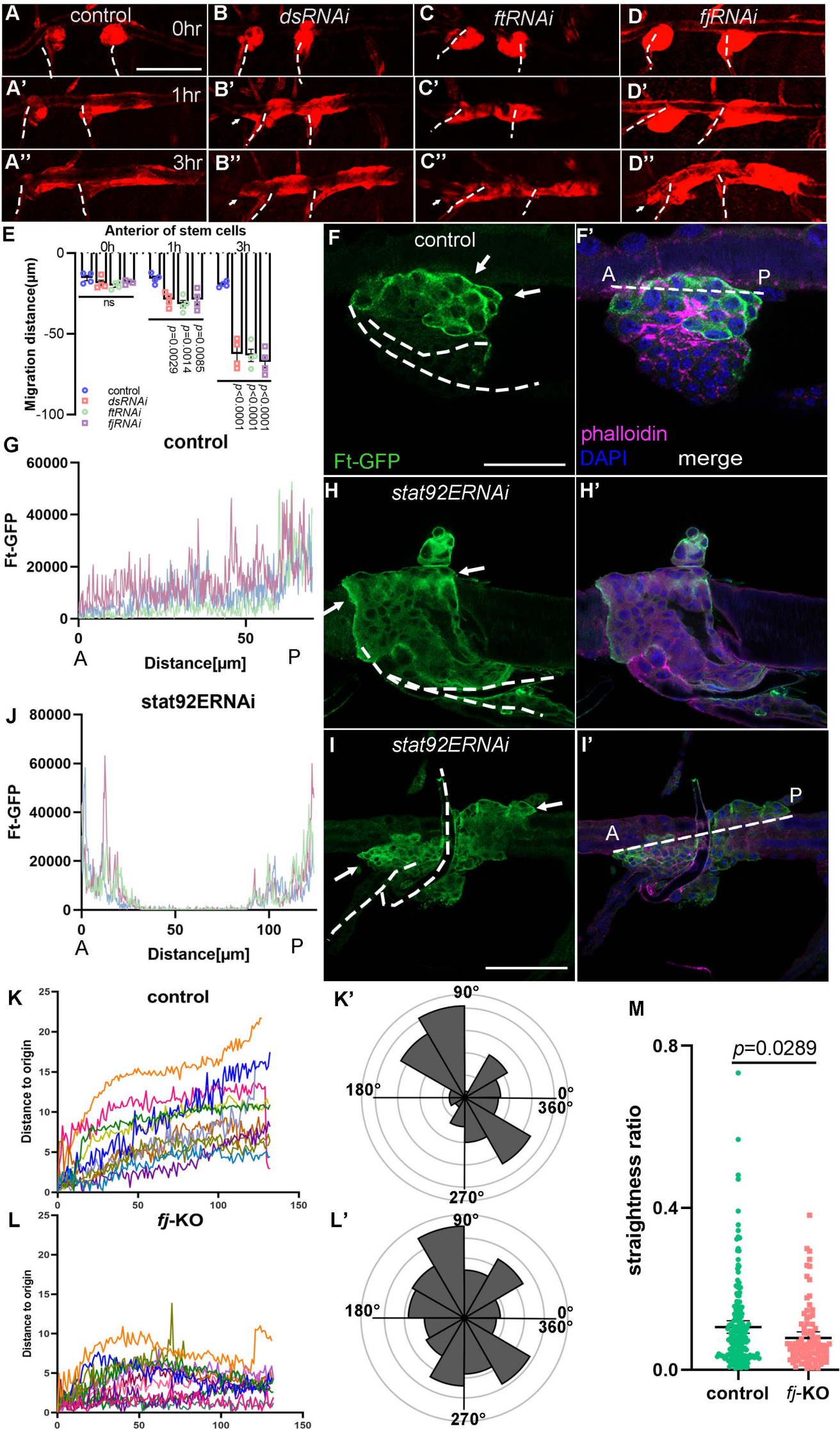
A
control
0hr
B
dsRNAi
C
ftRNAi
D
fjRNAi
A'
1hr
B'
C'
D'
A''
3hr
B''
C''
D''
E
Anterior of stem cells
0h
1h
3h
Migration distance(μm)
0
-50
-100
ns
p=0.0029
p=0.0014
p=0.0085
p<0.0001
p<0.0001
p<0.0001
control
dsRNAi
ftRNAi
fjRNAi
F
control
Ft-GFP
F'
A
P
phalloidin
DAPI
merge
G
control
Ft-GFP
60000
40000
20000
0
0
50
A
Distance[μm]
P
H
stat92ERNAi
H'
J
stat92ERNAi
Ft-GFP
80000
60000
40000
20000
0
0
50
100
A
Distance[μm]
P
I
stat92ERNAi
I'
A
P
K
control
Distance to origin
25
20
15
10
5
0
0
50
100
150
K'
90°
180°
0°
360°
270°
M
p=0.0289
straightness ratio
0.8
0.4
0.0
control
fj-KO
L
fj-KO
Distance to origin
25
20
15
10
5
0
0
50
100
150
L'
90°
180°
0°
360°
270°

Figure 6

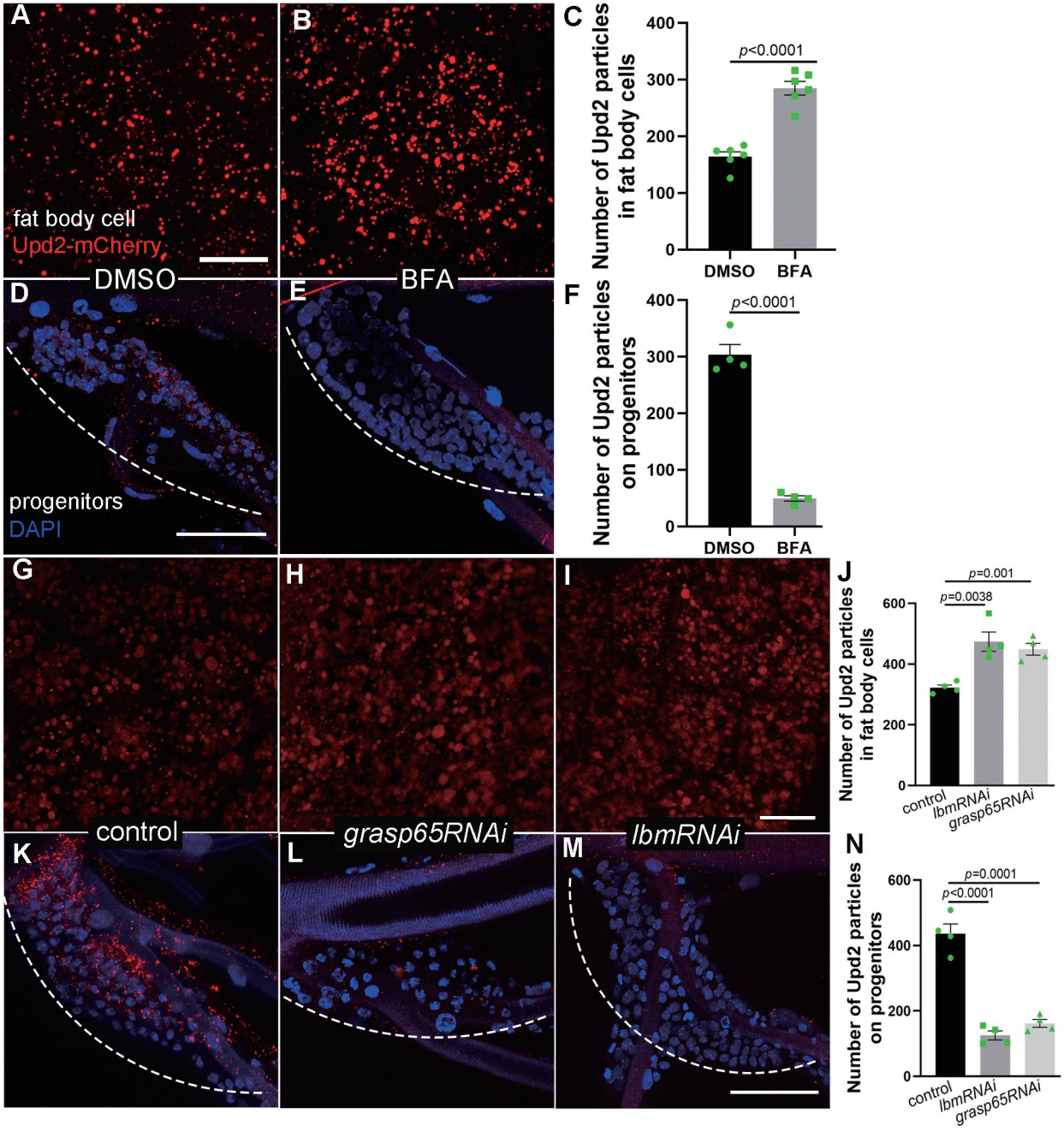
A
B
fat body cell
Upd2-mCherry
DMSO
BFA
C
Number of Upd2 particles in fat body cells
p<0.0001
400
300
200
100
0
DMSO
BFA
D
E
progenitors
DAPI
F
Number of Upd2 particles on progenitors
p<0.0001
400
300
200
100
0
DMSO
BFA
G
H
I
control
grasp65RNAi
lbmRNAi
J
Number of Upd2 particles in fat body cells
p=0.001
p=0.0038
600
400
200
0
control
lbmRNAi
grasp65RNAi
K
L
M
N
Number of Upd2 particles on progenitors
p=0.0001
p<0.0001
600
400
200
0
control
lbmRNAi
grasp65RNAi

Figure 7

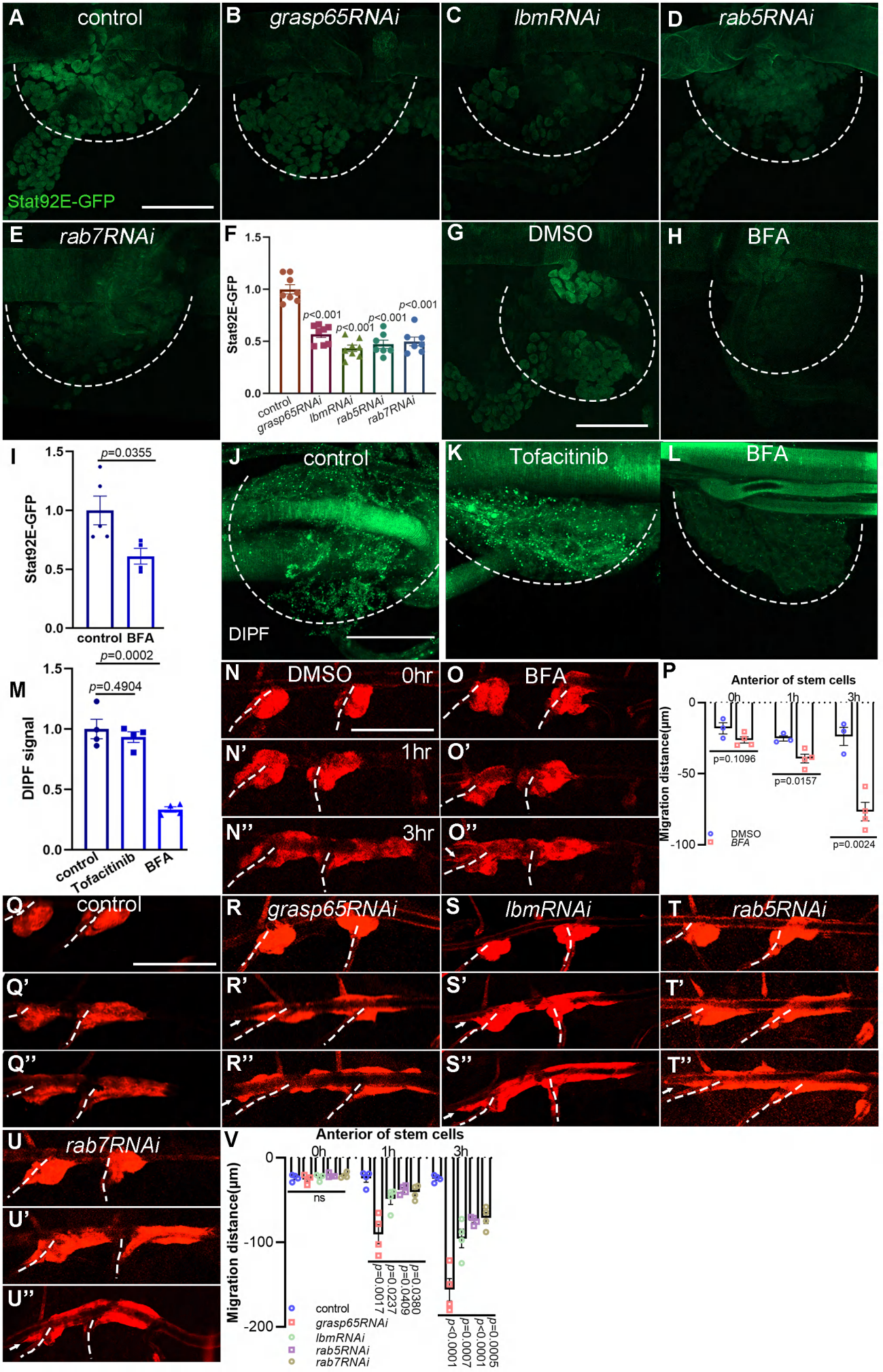
A control
Stat92E-GFP
B grasp65RNAi
C lbmRNAi
D rab5RNAi
E rab7RNAi
F
Stat92E-GFP
1.5
1.0
0.5
0.0
p<0.001
p<0.001
p<0.001
p<0.001
control
grasp65RNAi
lbmRNAi
rab5RNAi
rab7RNAi
G DMSO
H BFA
I
p=0.0355
Stat92E-GFP
control BFA
J control
DIPF
K Tofacitinib
L BFA
M
p=0.0002
p=0.4904
DIPF signal
control
Tofacitinib
BFA
N DMSO 0hr
N' 1hr
N'' 3hr
O BFA
O'
O''
P
Anterior of stem cells
0h
1h
3h
Migration distance(μm)
0
-50
-100
p=0.1096
p=0.0157
p=0.0024
DMSO
BFA
Q control
Q'
Q''
R grasp65RNAi
R'
R''
S lbmRNAi
S'
S''
T rab5RNAi
T'
T''
U rab7RNAi
U'
U''
V
Anterior of stem cells
0h
1h
3h
Migration distance(μm)
0
-100
-200
ns
p=0.0017
p=0.0237
p=0.0409
p=0.0380
p<0.0001
p=0.0007
p<0.0001
p=0.0005
control
grasp65RNAi
lbmRNAi
rab5RNAi
rab7RNAi

Figure 8

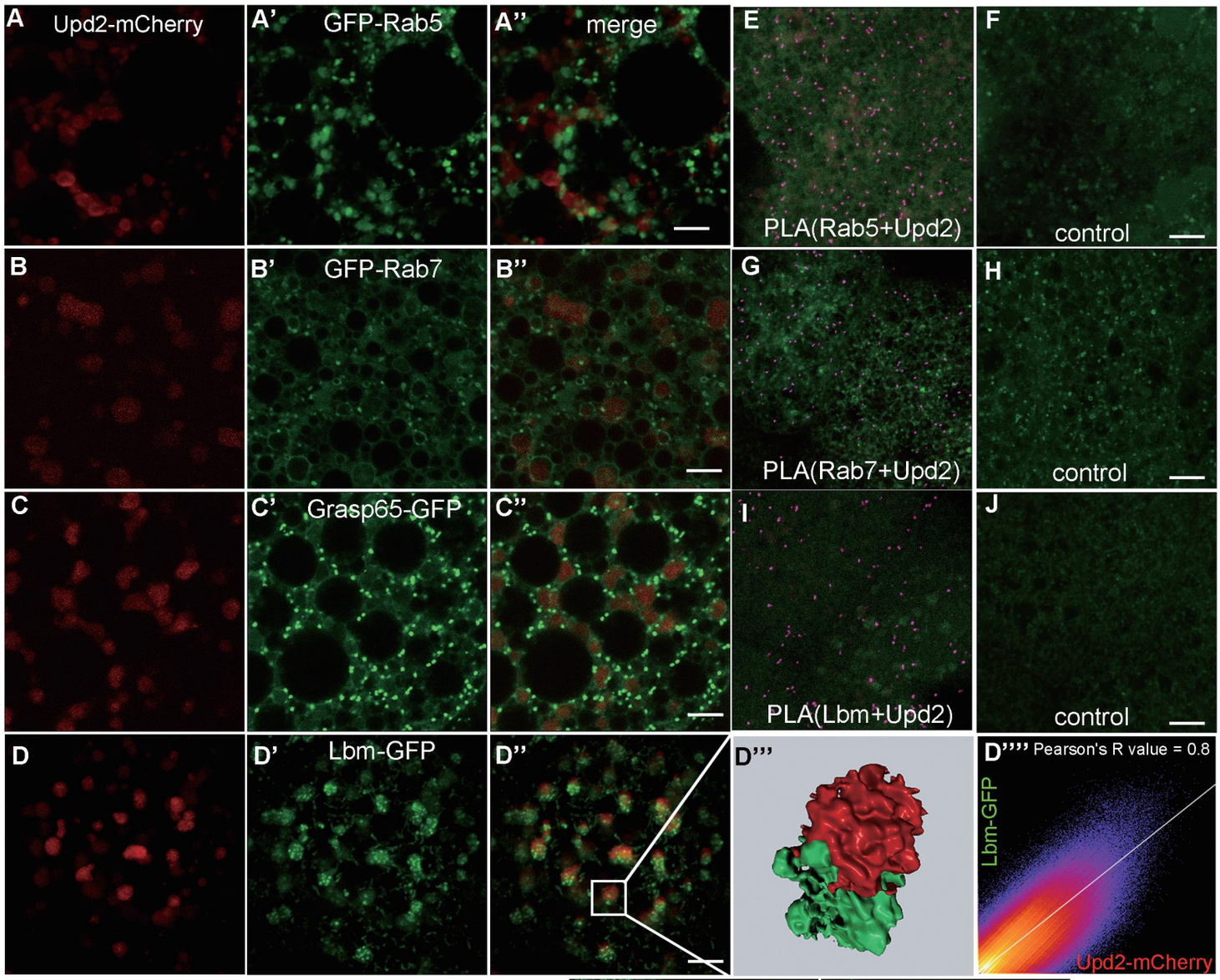
A
Upd2-mCherry
A'
GFP-Rab5
A''
merge
E
PLA(Rab5+Upd2)
F
control
B
B'
GFP-Rab7
B''
G
PLA(Rab7+Upd2)
H
control
C
C'
Grasp65-GFP
C''
I
PLA(Lbm+Upd2)
J
control
D
D'
Lbm-GFP
D''
D'''
D'''' Pearson's R value = 0.8
Lbm-GFP
Upd2-mCherry

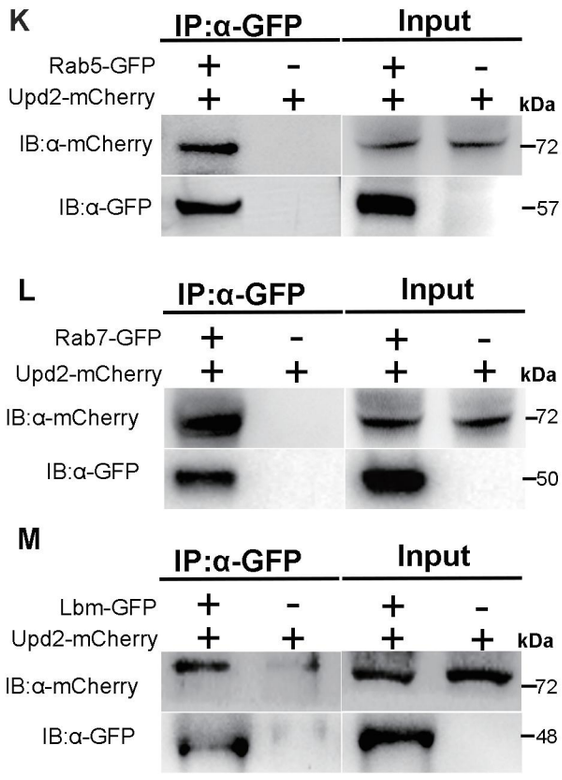
K
IP:α-GFP
Input
Rab5-GFP
Upd2-mCherry
kDa
IB:α-mCherry
IB:α-GFP
72
57
L
IP:α-GFP
Input
Rab7-GFP
Upd2-mCherry
kDa
IB:α-mCherry
IB:α-GFP
72
50
M
IP:α-GFP
Input
Lbm-GFP
Upd2-mCherry
kDa
IB:α-mCherry
IB:α-GFP
72
48

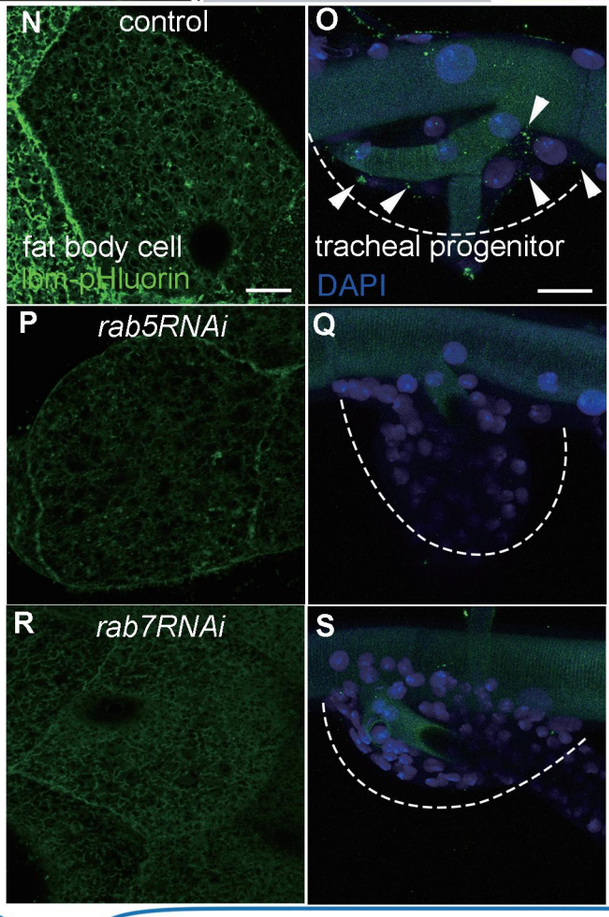
N
control
fat body cell
lbm-pHluorin
O
tracheal progenitor
DAPI
P
rab5RNAi
Q
R
rab7RNAi
S

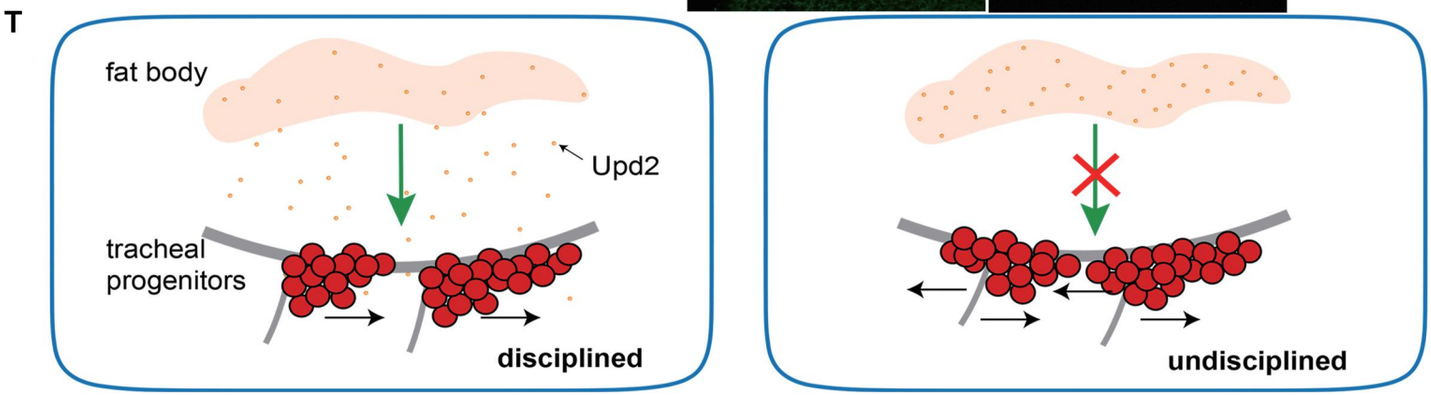
T
fat body
Upd2
tracheal progenitors
disciplined
undisciplined